ESC-TR-2007-075

Technical Report
1132

Clutter Cancellation Limits of Adaptive Processing Applied to Coherent Multiple-Input Multiple-Output Ground Moving Target Indication

L.L. Horowitz

31 August 2011

Lincoln Laboratory
MASSACHUSETTS INSTITUTE OF TECHNOLOGY
LEXINGTON, MASSACHUSETTS

Prepared for the Department of the Air Force under Air Force Contract FA8721-05-C-0002.

This report is based on studies performed at Lincoln Laboratory, a federally funded research and development center operated by Massachusetts Institute of Technology. This work was sponsored by the Department of the Air Force under Air Force Contract FA8721-05-C-0002.

The 66th Air Base Group Public Affairs Office has reviewed this report, and it is releasable to the National Technical Information Service, where it will be available to the general public, including foreign nationals.

This technical report has been reviewed and is approved for publication.

FOR THE COMMANDER

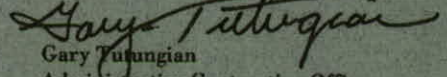

Gary Tutungian
Administrative Contracting Officer
Acquisition Enterprise Division

Massachusetts Institute of Technology
Lincoln Laboratory

Clutter Cancellation Limits of Adaptive Processing Applied to Coherent Multiple-Input Multiple-Output Ground Moving Target Indication

L.L. Horowitz
Group 103

Technical Report 1132

31 August 2011

Lexington Massachusetts

This page intentionally left blank.

EXECUTIVE SUMMARY

Coherent, multiple-input multiple-output (MIMO) extensions to radar systems offer a number of performance advantages over more conventional approaches. For ground moving target indication (GMTI), the benefits can include lower minimum detectable velocity (MDV) and more accurate target direction estimation. In part, these benefits are afforded by the superior clutter cancellation offered by the long, filled virtual array that MIMO can yield, while using relatively few physical antenna elements. In addition, the use of uncorrelated waveforms for coherent MIMO GMTI diffuses the transmitted energy uniformly over a broad azimuthal coverage region, yielding a long effective coherent integration time. This enhances the above benefits and also provides finer Doppler resolution. For applications in which the geometry and MIMO radar system design result in ground clutter occupying a suitably limited extent of range and Doppler, waveform sets such as time-division multiple access (TDMA) or Doppler-division multiple access (DDMA) can be used to realize the above benefits. However, it has been noted that the clutter cancellation is less effective when the clutter has a greater range-Doppler extent. Various alternative low-correlation waveform sets have failed to mitigate this problem.

In this report it is shown analytically that the extra difficulty of clutter cancellation referred to above is attributable to an unavoidable increase in the number of MIMO degrees of freedom required to cancel the ground clutter, when the clutter occupies an extended domain of range Doppler. Specifically, the following is a section-by-section synopsis of the discussion and results herein.

1. In the Introduction, time-domain computer simulation results are presented, showing how the signal-to-interference-plus-noise ratio (SINR) for MIMO GMTI is less than ideal for extended range domains of ground clutter. Specifically, practical waveforms chosen to have low cross-correlation functions over extended range domains are seen to result in significantly worse SINR than do hypothetical ideal waveforms. The ideal waveforms are simulated as having matching autocorrelation functions and zero cross-correlation functions. To explain this effect, a pictorial discussion is given, showing how matched filters (MF) for different waveforms effectively weight the complex clutter reflections from the ground with different correlation functions versus range. The different correlation functions result in decorrelation of the outputs of the filters matched to the different waveforms. In turn, this causes degradation of the ability to cancel the clutter returns when the matched-filter outputs are adaptively weighted for that purpose. The points made in this introductory section are quantified analytically in succeeding sections.

2. The assumptions, limitations, and applicability of the ensuing analytical results are discussed. The analysis considers cases in which the MIMO virtual array is critically spaced (i.e., $\lambda/2$) and filled. In particular, the results consider only the clutter on the "ray" isoDoppler to the

hypothesized target.[1] The most familiar interpretation, and that used in this Executive Summary, would be that the analytical results apply to a pulsed-Doppler paradigm, in which each waveform consists of a sequence of identical pulses over the coherent processing interval, and Doppler filtering (to focus on the hypothesized target Doppler) is performed after matched filtering and prior to adaptive weighting for clutter cancellation. However, a broader interpretation is that the waveforms are free to be of any form (pulsed or not), and the analysis shows the statistical structure of the clutter arising from just the most critical region on the ground (i.e., isoDoppler to the target).

3. A mathematical model is developed for the response of the MIMO receive antennas and MFs to the ray of clutter on the ground isoDoppler to the hypothesized target. Each of the R receivers is followed by T matched filters, corresponding to the T transmit waveforms. The RT outputs, sampled at the range of the hypothesized target and Doppler filtered to focus on the hypothesized target velocity, are adaptively weighted to cancel the clutter on the isoDop, while maintaining gain on the hypothesized target azimuth angle. The study considers the rank and eigenstructure of the RT × RT covariance matrix between the various received, processed outputs, as resulting just from the clutter on the isoDop ray on the ground. When more eigenvalues are positive, more degrees of freedom potentially need to be expended to cancel the ground clutter. In this section, it is shown that for uncorrelated signals, the frequency spectra cannot overlap and the autocorrelation functions are orthogonal to one another, which causes decorrelation of the ground clutter returns at the outputs of the MFs for the different signals. It follows that "ideal" waveform sets do not exist over an extended domain of range. This last fact was already known, but the extent of its impact on the ability to cancel clutter was not fully realized. The MIMO response to a point target is shown to have the familiar Vandermonde virtual-array characteristic of MIMO, while the response to clutter can have multiple modes. Also, it is shown how single-input multiple-output (SIMO) GMTI yields a clutter covariance having only one nonzero eigenvalue.

4. Under simple assumptions, it is shown that the MIMO clutter covariance has T equal, positive eigenvalues whenever the T waveforms are uncorrelated. This occurs independent of the direction of the ray of clutter isoDoppler to the target. This phenomenon is a worst case for clutter cancellation. Also, it is shown that in this case the receive array alone performs all clutter nulling for MIMO, for each transmitter separately. This makes MIMO and SIMO equivalent for clutter cancellation, in this respect.

---

[1] In some system designs with low-velocity platforms, there can occur hypothesized target velocities for which no isoDoppler clutter ray exists on the ground. Clutter cancellation may not be required in such cases. Also, if there are multiple rays isoDoppler to the target (i.e., Doppler ambiguities) within the azimuthal coverage region, clutter cancellation requires more degrees of freedom in order to place antenna array nulls in multiple directions. The analysis herein considers only cases in which a single isoDoppler clutter ray occurs.

5. For the case in which T = 2, a penalty function is derived, which evidences quadratic growth of the product of the highest two eigenvalues of the MIMO clutter covariance whenever the two signals are not proportional. This result relates directly to the size of the second eigenvalue of the covariance, which requires an extra degree of freedom for cancellation. The penalty emphasizes waveform differences at frequencies where the energy density spectrum of either waveform is high, suggesting the use of flat-spectrum waveforms. The following statement is also proven: For T = 2, the MIMO clutter covariance is of rank 1 or 0 for all ϕ if and only if (iff) the two waveforms are proportional. Here, ϕ is defined as the phase difference between adjacent transmitters, as would be seen on the ray of clutter isoDoppler to the target.

6. For arbitrary T, it is shown that the MIMO clutter covariance is of rank 1 or 0 for all ϕ iff the T × T waveform cross-correlation matrix as a function of delay satisfies the equality $C(\tau) = C(0)\gamma(\tau)$, for all relevant values of τ, for some scalar (autocorrelation) function, $\gamma(\tau)$. This property is called delay similarity of the waveform cross-correlation matrix. Using the above equivalence proves that the statement in (5) above is true for any value of T. Further, the properties of analytic functions then are used to extend the statement finally to the following pair of statements: (1) For any T, if all the waveforms are proportional then the MIMO clutter covariance is of rank 1 or 0 for all ϕ, and (2) for any T, if any pair of the T waveforms are not proportional, then the MIMO clutter covariance can have rank 1 or 0 only for isolated values of ϕ.

7. Three different potential techniques are examined briefly for improving the cancellation of clutter over extended domains. The three techniques are adaptively weighted slow-time taps (i.e., Space-Time Adaptive Processing, or STAP), adaptively weighted fast-time taps, and nonconventional reception (i.e., reception not constrained to use matched filters for the T waveforms). For uncorrelated MIMO waveforms, it is shown that none of these techniques addresses the basic decorrelation problem of the MIMO clutter covariance. Thus, while these techniques could improve performance somewhat, they are not expected to restore near-ideal performance.

8. For clutter occupying only a suitably limited domain of range Doppler, it is already known that near-ideal clutter cancellation can be achieved through appropriate waveform design, as noted above. Using the example of TDMA waveforms, one can show here that it is possible to achieve the delay-similarity property defined in (6) above when the clutter occupies only a suitably limited domain, which implies that the MIMO clutter covariance will have rank 1 or 0 for all ϕ. Thus, ideal sets of waveforms do exist for suitably limited domains of clutter. This agrees with the near-ideal performance that has been observed in computer simulations using TDMA (or DDMA) waveforms in scenarios having limited domains of clutter. For TDMA, the cases in which the clutter is suitably limited are defined in terms of the MIMO radar system design, involving the velocity of the platform, the center frequency, the azimuth and

elevation footprint of the transmit and receive antennas, the number of transmitters, and the duty cycle. For clutter exceeding such limited domains, the best design of MIMO waveforms for minimal degradation of clutter cancellation and other beneficial properties remains an open issue. Airborne experimental data will be used to assess the resulting performance.

ACKNOWLEDGMENTS

When Dan Bliss asked me to analyze why computer simulations of MIMO GMTI yielded less-than-ideal performance under some circumstances, it was my hope to find an easy cure for the problem. I had no desire to prove that the performance degradation was inherent in the concept of using uncorrelated signals for MIMO GMTI when the ground clutter occupied an extended domain. The excellent results that Dan and his team had obtained previously for various applications of MIMO technology caused me to feel sorry that the GMTI application refused to yield all of the desired performance attributes. Nonetheless, the MIMO team of Dan, Keith Forsythe, Dan Rabideau, Shakti Davis, Shawn Kraut, and Glenn Fawcett gave me excellent, helpful technical feedback as I presented my latest results at our weekly meetings. For this I am very grateful. In particular, the proof concept involving the theory of analytic functions in Section 6 was obtained from Keith Forsythe, and the computer simulations were run by Glenn Fawcett, using a simulation designed by Shakti Davis. The manuscript was painstakingly prepared by Pamela O'Connor and Loretta Wesley, with unsurpassed accuracy.

This page intentionally left blank.

TABLE OF CONTENTS

		Page
	Executive Summary	iii
	Acknowledgments	vii
1.	INTRODUCTION	1
2.	ASSUMPTIONS, LIMITATIONS, AND APPLICABILITY OF ANALYTICAL RESULTS	11
3.	MATHEMATICAL MODEL FOR MIMO GMTI OBSERVATIONS	13
4.	MIMO CLUTTER COVARIANCE FOR UNCORRELATED WAVEFORMS	23
5.	IMPACT OF UNEQUAL WAVEFORMS ON THE SECOND EIGENVALUE OF THE MIMO CLUTTER COVARIANCE, WHEN T = 2	25
6.	IMPACT OF UNEQUAL WAVEFORMS ON THE SECOND EIGENVALUE OF THE MIMO CLUTTER COVARIANCE, WHEN T > 2	35
7.	PROSPECTS FOR IMPROVING THE CANCELLATION OF CLUTTER OVER EXTENDED DOMAINS	45
8.	BENEFITS OF A LIMITED RANGE-DOPPLER DOMAIN OF CLUTTER	49
9.	SUMMARY	53
	References	55

This page intentionally left blank.

LIST OF ILLUSTRATIONS

Figure No.		Page No.
1.1	Primary ground clutter regions for GMTI (single-transmitter case).	2
1.2	Ground clutter region for analysis (single-transmitter case).	3
1.3	Adaptive gain pattern (single-transmitter case).	4
1.4	Computer simulation results using ideal MIMO waveforms in a sample scenario.	5
1.5	Reception for MIMO GMTI (3-transmitter case).	6
1.6	Realistic, low-correlation waveforms ("Wolf Whistles") yield poorer SINR performance than ideal MIMO waveforms.	7
3.1	MIMO transmission and reception.	13
4.1	The blue curve repeats results from Figure 1.6, with closely spaced receivers.	24
5.1	Pythagorean theorem in L_2 function space.	28
6.1	Equivalence of conditions.	35
8.1	TDMA waveforms and correlation functions.	50

This page intentionally left blank.

1. INTRODUCTION

Coherent, multiple-input multiple-output (MIMO) extensions to radar systems offer a number of performance advantages over more conventional approaches [1–11]. For ground moving target indication (GMTI), the benefits can include lower minimum detectable velocity (MDV) [1, 3, 8, 9] and more accurate target direction estimation [1, 3]. In part, these benefits are afforded by the superior clutter cancellation offered by the long filled virtual array that MIMO can yield, while using relatively few physical antenna elements [1, 3, 8]. In addition, the use of uncorrelated waveforms [12–14] for coherent MIMO GMTI diffuses the transmitted energy uniformly over a broad azimuthal coverage region, yielding a long effective coherent integration time [3, 8]. This enhances the above benefits and also provides finer Doppler resolution. For applications in which the geometry and MIMO radar system design result in ground clutter occupying a suitably limited extent of range and Doppler, waveform sets such as time-division multiple access (TDMA) or Doppler-division multiple access (DDMA) can be used to realize the above benefits [3, 15]. However, it has been noted that the clutter cancellation is less effective when the clutter has a greater range-Doppler extent [3, 15, 16]. Various alternative low-correlation waveform sets have failed to mitigate this problem [3, 15, 16].

In this report it is shown analytically that the extra difficulty of clutter cancellation referred to above is attributable to an unavoidable increase in the number of MIMO degrees of freedom required to cancel the ground clutter, when the clutter occupies an extended domain of range Doppler. To explain this effect, a pictorial discussion is given in this Introduction, showing how matched filters (MF) for different waveforms effectively weight the complex clutter reflections from the ground with different correlation functions versus range. The different correlation functions result in decorrelation of the outputs of the filters matched to the different waveforms. In turn, this causes degradation of the ability to cancel the clutter returns when the matched-filter outputs are adaptively weighted for that purpose. Time-domain computer simulation results are presented [16], showing how the signal-to-interference-plus-noise ratio (SINR) for MIMO GMTI is less than ideal for extended range domains of ground clutter. Specifically, practical waveforms chosen to have low cross-correlation functions over extended range domains are seen to result in significantly worse SINR than do hypothetical ideal waveforms. The ideal waveforms are simulated as having matching autocorrelation functions and zero cross-correlation functions.

Figure 1.1 depicts the antenna footprint on the ground, for an ordinary single-transmitter GMTI radar. The regions of clutter on the ground experiencing the highest system gain will be examined. The radar is assumed to fly horizontally across the bottom of the diagram. The range and azimuth variations on the ground are as indicated. The location of a hypothesized target is shown in blue. The target has a hypothesized range, azimuth, and radial velocity. At the lower left, the initial stages of the receive signal processing are depicted. The signal processing is intended to focus each antenna output on the range and Doppler of the hypothesized target. This causes specific regions on the ground to experience high system gain. The matched filters (MFs) all focus on the target range, and their peak response is shown in green in the figure. The Doppler beam formers focus the MF outputs on the hypothesized Doppler of the target,

and their peak response on the stationary ground is shown in red (a "ray"). Note that the ground experiencing the highest gain is not at the same azimuth angle as the target. This is because the target is hypothesized to be moving radially, so the ground in the direction of the target does not have the same Doppler shift as the target does; hence it does not receive peak gain as the target does. When the hypothesized Doppler of the target is changed, the azimuth angle of the clutter isoDoppler to the target also changes, approaching the angle of the target as the hypothesized radial velocity of the target relative to the ground approaches zero. The ground region receiving the highest overall gain is shown in gold; it is the intersection of the peak range response of the MFs and the peak Doppler response of the Doppler beam focused on the target.

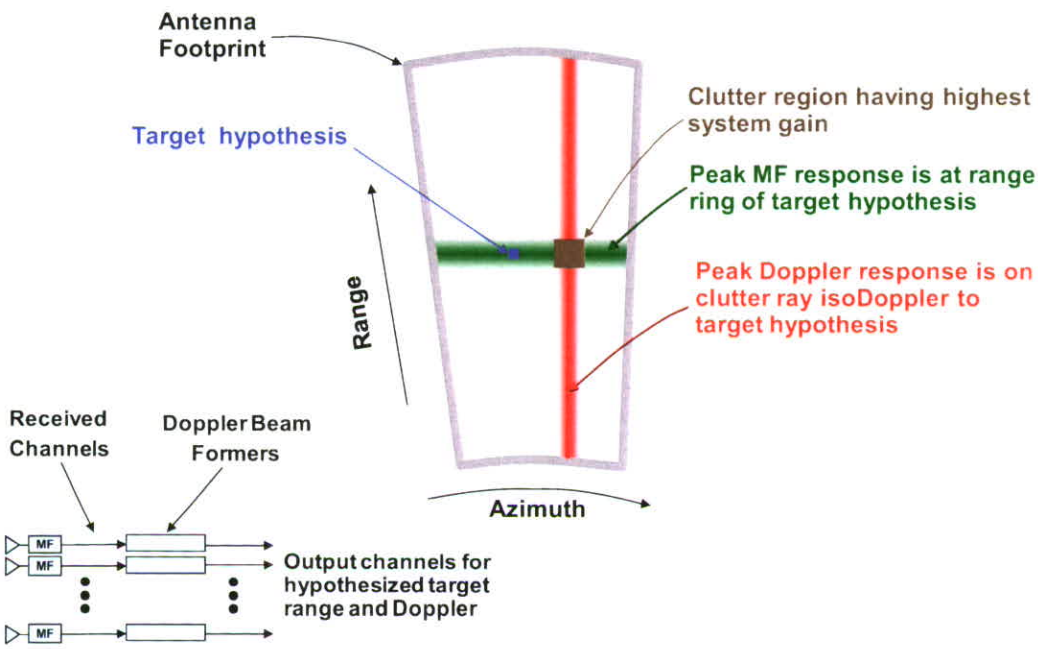

Figure 1.1. Primary ground clutter regions for GMTI (single-transmitter case).

The region of ground clutter that is the focus of the analysis is shown in Figure 1.2. This is the clutter ray (in red) isoDoppler to the hypothesized target. Here is depicted (in green) the (complex) correlation response of the MFs, peaking at the hypothesized target range [17, pp. 32–33]. The correlation response weights the reflectivities of patches of ground on the clutter ray. This occurs in each antenna output channel, as mentioned above.

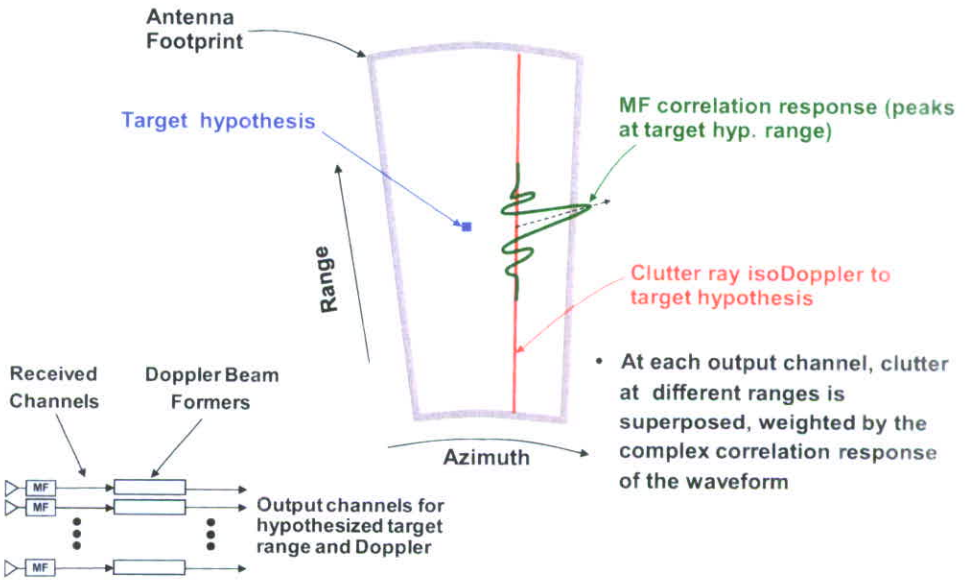

Figure 1.2. Ground clutter region for analysis (single-transmitter case).

The next step in the processing is to combine the outputs of the antennas in an adaptive manner, to cancel the clutter. This is depicted in Figure 1.3. The array gain pattern versus azimuth angle is depicted in red at the bottom of the diagram. The gain is lower in the direction of the clutter ray and higher in the direction of the target. If the hypothesized target had a lower velocity (relative to the ground) than shown in Figure 1.3, then the clutter isoDoppler to the target would be at a closer angle to the target. This would reduce the ability of the array to form an adaptive null on the angle of the clutter ray while maintaining gain on the angle of the target. Figure 1.4 shows computer simulation results [16] for the SINR that would be achieved in a sample scenario (see details on figure). The abscissa shows the normalized Doppler [18, p. 13] of the hypothesized target, relative to the ground. The ordinate shows the SINR loss, in dB, relative to a clutter-free case. The loss is worst at 0 normalized Doppler, when the clutter isoDoppler to the target is at the same angle as the target and thus cannot be nulled relative to the target through adaptive weighting of the antenna outputs. The result shown is basically the same for two different radar system structures. One is the single-input multiple-output (SIMO) structure with a 25-element receive array at ($\lambda/2$) (i.e., critical) spacing. The second is a 5-transmitter, 5-receiver MIMO array, with ideal waveforms simulated, as noted on the figure. The virtual array for MIMO also has 25 elements, at ($\lambda/2$) spacing[2]. The simulation results are basically the same whether the critically sampled virtual array is achieved by using

[2] The locations of the antenna elements of the MIMO virtual array are the result of the convolution of the transmit element locations with the receive element locations [1, 3, 8].

receivers at ($\lambda/2$) spacing and transmitters at ($5\lambda/2$) spacing, or the reverse. The reasons that these three cases are equivalent will be discussed in Section 6, relative to (6.28). Incidentally, if the ground clutter had an extended Doppler domain (e.g., due to a high-velocity platform), then there would be multiple rays of clutter on the ground (i.e., Doppler ambiguities). Those rays would each require cancellation, increasing the rank of the MIMO clutter covariance matrix. This topic arises again in Section 8. In Figure 1.3, the ability to cancel the clutter effectively depends on the antenna outputs having high channel-to-channel correlation for the clutter. The fact that the channels utilized identical MFs in the SIMO case has ensured that the weighting functions on the ground are identical on the clutter ray. This maintains high correlation between channels, hence effective clutter cancellation.

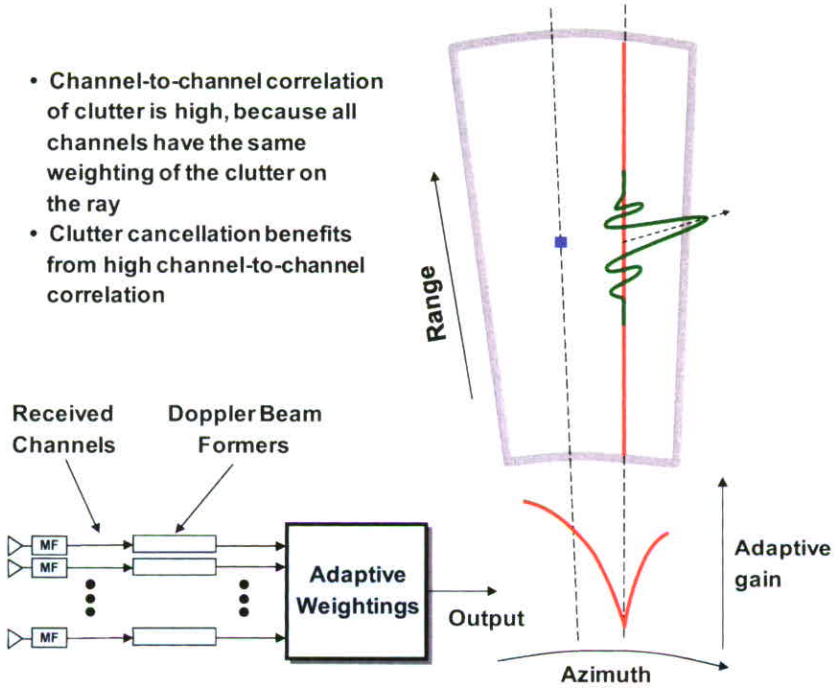

Figure 1.3. Adaptive gain pattern (single-transmitter case).

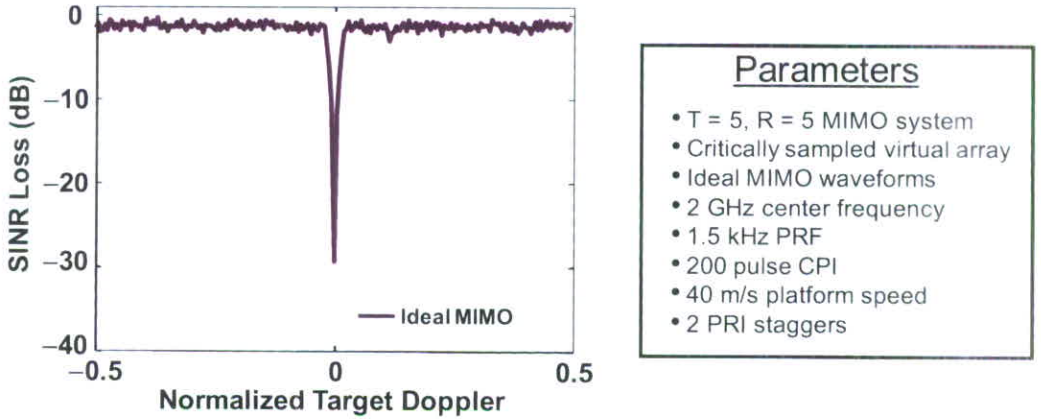

Figure 1.4. Computer simulation results using ideal MIMO waveforms in a sample scenario. Note that all simulation results in this report utilize 2 pulse-repetition-interval (PRI) staggers [18, p. 125], for somewhat improved performance over simple post-Doppler, angle-only adaptivity, which is analyzed in the text.

In contrast, the situation for MIMO reception using realistic waveforms is now examined. Figure 1.5 depicts reception for a 3-transmitter case. More details of the signal processing structure are given in Section 3. Each receiving antenna is followed by three MFs, one for each waveform. For any antenna, the weighting of the clutter at the output of MF1 depends on the autocorrelation function of waveform #1 and on its cross-correlation functions with waveforms #2 and #3. Unless the waveforms are the same, it turns out (as proven in Section 6) that the clutter on the ray is not weighted identically at the three MF outputs, causing a loss of correlation (this can be avoided when the clutter occupies only a limited domain of range Doppler, as discussed in Section 8). This limits the ability to cancel the clutter. In fact, if the three waveforms were fully uncorrelated (at all delays), then the MIMO clutter covariance would have 3 equal eigenvalues, requiring 3 degrees of freedom to cancel the clutter (see Section 4). This is in contrast to the 1-transmitter case discussed above, in which all the MF outputs would have high correlation, and the clutter covariance in theory could have rank 1, as discussed in Section 3. The performance impact of using realistic low-correlation MIMO waveforms is seen in Figure 1.6 [16]. The result for a MIMO system with a specific set of low-correlation waveforms ("Wolf Whistles") have been added to the results for ideal waveforms from Figure 1.4. The width of the SINR notch around 0 normalized Doppler has clearly increased. The extra wiggle in the SINR loss curve at normalized

Doppler near 0.1 is due to an extra target in the training data for the adaptive weights[3]. A number of low-correlation waveform sets have been tried [16], with similar results to those in Figure 1.6. In this particular case, the five receivers had ($\lambda/2$) spacing, and the transmitters had ($5\lambda/2$) spacing. In Section 4, the (significant) impact of reversing the transmitters and receivers for realistic waveforms will be discussed.

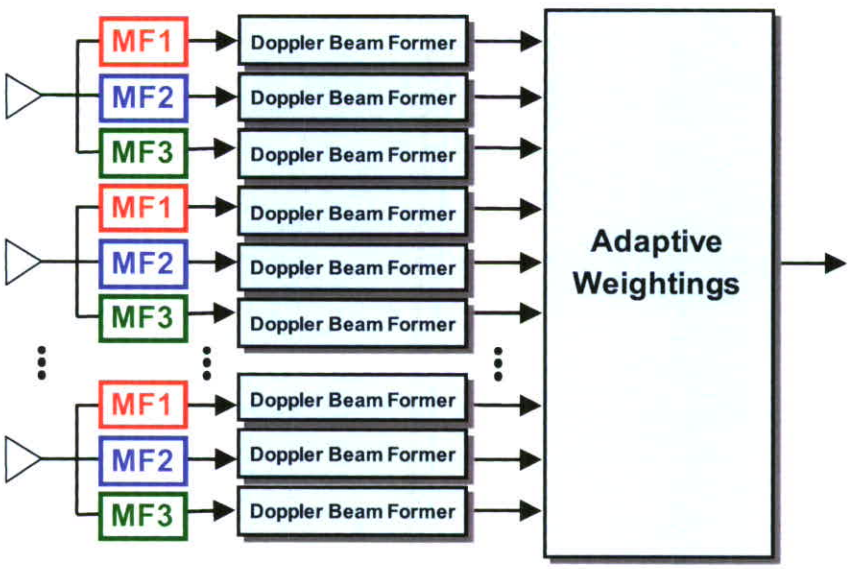

Figure 1.5. Reception for MIMO GMTI (3-transmitter case).

[3] The time-domain GMTI simulation included clutter, receiver noise, and also 5 moving targets, having various ranges, azimuths, and velocities. The sample covariance matrix used to form the adaptive weights was trained by sampling the outputs of the Doppler beam formers (see Figure 1.5) at the normalized Doppler frequency of the target hypothesis. Training samples were taken at a set of 300 range bins, not including the range bin of the target hypothesis (to prevent self-nulling). In the case shown in Figure 1.6, an actual target was located in one of the range bins used for training. When the normalized Doppler frequency of the hypothesized target equaled that of the actual target, the sample covariance matrix contained significant power from the actual target. This forced an array null to be formed on the angle of the actual target, in addition to the null on the clutter ray isoDoppler to the target hypothesis. The formation of two nulls required two degrees of freedom, for ideal waveforms. However, more degrees of freedom were required for realistic, low-correlation waveforms, causing the extra wiggle in the SINR loss curve in Figure 1.6, at the normalized Doppler frequency of the actual target in the training data.

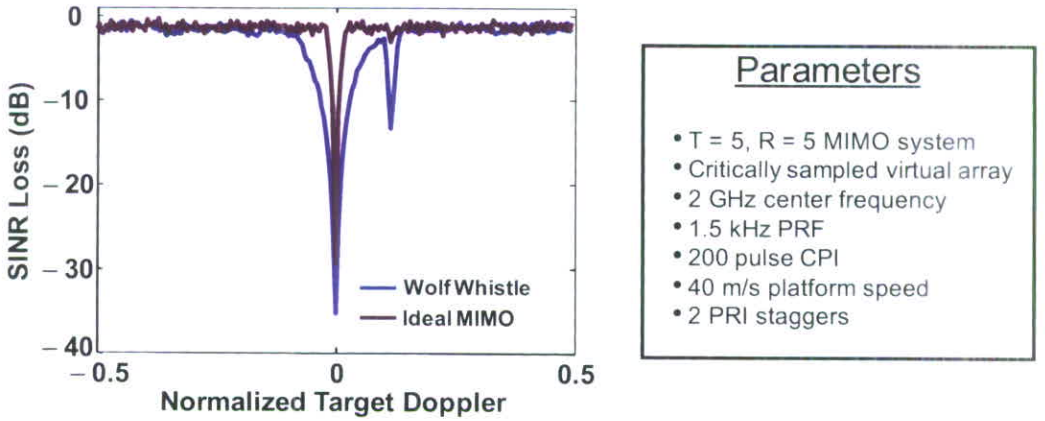

Figure 1.6. Realistic, low-correlation waveforms ("Wolf Whistles") yield poorer SINR performance than ideal MIMO waveforms.

The points made in this introductory section are quantified analytically in Sections 2 through 6. Sections 7 and 8 introduce additional topics. Specifically, the following is a section-by-section synopsis of the discussion and results in this report:

1. Introduction—this section.

2. The assumptions, limitations, and applicability of the ensuing analytical results are discussed. The analysis considers cases in which the MIMO virtual array is critically spaced and filled. In particular, the results consider only the clutter on the ray isoDoppler to the hypothesized target.[4] The most familiar interpretation, and that used in this Introduction, would be that the analytical results apply to a pulsed-Doppler paradigm, where each waveform consists of a sequence of identical pulses over the coherent processing interval, and Doppler filtering (to focus on the hypothesized target Doppler) is performed after matched filtering and prior to adaptive weighting for clutter cancellation (i.e., post-Doppler clutter cancellation [18]). However, a broader interpretation is that the waveforms are free to be of any form (pulsed or not), and the analysis here shows the statistical structure of the clutter arising from just the most critical region on the ground (i.e., isoDoppler to the target).

[4] In some system designs with low-velocity platforms, there can occur hypothesized target velocities for which no isoDoppler clutter ray exists on the ground [18, p. 27]. Clutter cancellation may not be required in such cases. Also, if there are multiple rays isoDoppler to the target (i.e., Doppler ambiguities) within the azimuthal coverage region, clutter cancellation requires more degrees of freedom in order to place antenna array nulls in multiple directions. The analysis herein considers only cases in which a single isoDoppler clutter ray occurs.

3. A mathematical model is developed for the response of the MIMO receive antennas and MFs to the ray of clutter on the ground isoDoppler to the hypothesized target. Each of the R receivers is followed by T matched filters, corresponding to the T transmit waveforms. The RT outputs, sampled at the range of the hypothesized target and Doppler filtered to focus on the hypothesized target velocity, are adaptively weighted to cancel the clutter on the isoDop while maintaining gain on the hypothesized target azimuth angle. The study considers the rank and eigenstructure of the RT × RT covariance matrix between the various received, processed outputs, as resulting just from the clutter on the isoDop ray on the ground. When more eigenvalues are positive, more degrees of freedom potentially need to be expended to cancel the ground clutter. Any performance degradation from training the adaptive system to learn this covariance is ignored here (i.e., the covariance is assumed to be known). As noted above, finite training data is used in the computer simulation results. In this section, it is shown that for uncorrelated signals, the frequency spectra cannot overlap and the autocorrelation functions are orthogonal to one another, which causes decorrelation of the ground clutter returns at the outputs of the MFs for the different signals. It follows that ideal waveform sets do not exist over an extended domain of range. This last fact was already known [19], but the extent of its impact on the ability to cancel clutter was not fully realized. The MIMO response to a point target is shown to have the familiar Vandermonde virtual-array characteristic of MIMO, while the response to clutter can have multiple modes. Also, it is shown how single-input multiple-output (SIMO) GMTI yields a clutter covariance having only one nonzero eigenvalue.

4. Under simple assumptions, it is shown that the MIMO clutter covariance has T equal, positive eigenvalues whenever the T waveforms are uncorrelated. This occurs independent of the direction of the ray of clutter isoDoppler to the target. This phenomenon is a worst case for clutter cancellation. Also, it is shown that in this case the receive array alone performs all clutter nulling for MIMO, for each transmitter separately. This makes MIMO and SIMO equivalent for clutter cancellation, in this respect.

5. For the case where T = 2, a penalty function is derived, evidencing quadratic growth of the product of the highest two eigenvalues of the MIMO clutter covariance whenever the two signals are not proportional. This result relates directly to the size of the second eigenvalue of the covariance, which requires an extra degree of freedom for clutter cancellation. The penalty emphasizes waveform differences at frequencies where the energy density spectrum of either waveform is high, suggesting the use of flat-spectrum waveforms. The following statement is also proven: For T = 2, the MIMO clutter covariance is of rank 1 or 0 for all ϕ if and only if (iff) the two waveforms are proportional. Here, ϕ is defined as the phase difference between adjacent transmitters, as would be seen on the ray of clutter isoDoppler to the target.

6. For arbitrary T, it is shown that the MIMO clutter covariance is of rank 1 or 0 for all ϕ iff the T × T waveform cross-correlation matrix as a function of delay satisfies the equality $C(\tau) = C(0)\gamma(\tau)$, for all relevant values of τ, for some scalar (autocorrelation) function,

$\gamma(\tau)$. This property is called delay similarity of the waveform cross-correlation matrix. Using the above equivalence proves that the statement following the colon in (5) above is true for any value of T. Further, the properties of analytic functions then are used to extend the statement finally to the following pair of statements: (1) For any T, if all the waveforms are proportional, then the MIMO clutter covariance is of rank 1 or 0 for all ϕ, and (2) for any T, if any pair of the T waveforms are not proportional, then the MIMO clutter covariance can have rank 1 or 0 only for isolated values of ϕ.

7. Three different potential techniques are examined briefly for improving the cancellation of clutter over extended domains. The three techniques are adaptively weighted slow-time taps (i.e., Space-Time Adaptive Processing [STAP] [18]), adaptively weighted fast-time taps and nonconventional reception (i.e., reception not constrained to use matched filters for the T waveforms). For uncorrelated MIMO waveforms, it is shown that none of these techniques addresses the basic decorrelation problem of the MIMO clutter covariance. Thus, while these techniques could improve performance somewhat, they are not expected to restore near-ideal performance.

8. For clutter occupying only a suitably limited domain of range Doppler, it is already known that near-ideal clutter cancellation can be achieved through appropriate waveform design, as noted above. Using the example of TDMA waveforms, one can show here that it is possible to achieve the delay-similarity property defined in (6) above when the clutter occupies only a suitably limited domain, which implies that the MIMO clutter covariance will have rank 1 or 0 for all ϕ. Thus, ideal sets of waveforms do exist for suitably limited domains of clutter. This agrees with the near-ideal performance that has been observed in computer simulations using TDMA (or DDMA) waveforms in scenarios having limited domains of clutter [16]. For TDMA, the cases in which the clutter is suitably limited are defined in terms of the MIMO radar system design, involving the velocity of the platform, the center frequency, the azimuth and elevation footprint of the transmit and receive antennas, the number of transmitters, and the duty cycle. For clutter exceeding such limited domains, the best design of MIMO waveforms for minimal degradation of clutter cancellation and other beneficial properties remains an open issue. Airborne experimental data will be used to assess the resulting performance.

9. Summary.

Note that [15] examined the difficulties of waveform selection posed by clutter of unlimited range or Doppler extents for a restricted situation (i.e., 2 transmitters, 1 receiver) and suggested some MIMO waveforms for use in applications in which the range and Doppler extents of the clutter are limited. The work herein extends the conclusions of [15] to an arbitrary number of transmitters and receivers, and quantifies the diffusion of power into multiple eigenvalues of the MIMO clutter covariance.

This page intentionally left blank.

2. ASSUMPTIONS, LIMITATIONS, AND APPLICABILITY OF ANALYTICAL RESULTS

To generate insight herein, the GMTI scenario and the MIMO design are kept simple, and only the primary contributing clutter is considered in the analysis. The MIMO waveforms are considered to be narrowband, and only far-field ground reflections are considered. The transmitters are assumed to transmit for a single coherent processing interval. The platform is assumed to fly in a direction parallel to the linear array of transmitters and receivers (sensors) with no yaw or pitch rotation. This keeps the geometry of the clutter simple on the ground, in terms of its Doppler shift versus the cone angle off the sensor array axis. The clutter having the same Doppler shift as the target hypothesis is approximated as forming a thin locus on the ground, at constant cone angle (it will be called a ray). Only that clutter ray is considered in the analysis. This same approximation was made in [15]; it allows attention to be focused on the limitations to clutter cancellation arising merely from the range extent of the clutter on the primary ray. As pointed out in the Introduction, the analysis considers only the cases in which there is exactly one such ray of clutter isoDoppler to the target, for the target velocity of interest. To obtain insight, one approximates the clutter ray as extending on both sides of the hypothesized target range, to distances beyond that corresponding to the finite coherent processing interval of the radar. For the mathematical model, this is equivalent to an unbounded extent of clutter in range, both positive and negative, from the range hypothesized for the target. In Section 8, however, clutter of bounded extent is discussed, as could occur because of the impact of antenna footprints or of the finite propagation horizon of the earth. As mentioned in Section 1, near-ideal SINR performance can be achieved when the clutter is of sufficiently bounded extent. Section 8 will show why this is true, in terms of the conceptualization developed herein.

The physical array of sensors has equally spaced transmitters and equally spaced receivers, configured to yield a critically sampled virtual array (see Section 3). Either the T transmitters or R receivers can be placed farther apart (details will be given below). For the MIMO system, each receiver is followed by a matched filter for each transmitted waveform, sampled at the range bin of the target hypothesis. This yields RT outputs for the range bin.

Because attention is restricted to a thin ray of clutter isoDoppler to the target, the analysis applies when viewed from either of two perspectives. On the one hand, it can be assumed that a repetitive pulsed-Doppler radar waveform structure has been imposed on all the waveforms, and that the matched-filter outputs have each been Doppler filtered to leave just the clutter isoDoppler to the target. Angle-only clutter cancellation is then applied to the RT outputs for the Doppler bin. The analytical results herein then apply to the (RT $\times$ RT) MIMO clutter covariance. The possibility for performance improvement in practice by using Space-Time Array Processing (STAP) [18] is discussed in Section 7. On the other hand, the restriction of consideration to just the thin ray of clutter isoDoppler to the target can be seen as providing free Doppler filtering, hence allowing a broader class of waveforms to be considered. Again, the clutter cancellation is based on the RT outputs, and the analytical results herein apply to the

covariance matrix of those outputs. Seen from this broader perspective, the negative predictions stated in Section 1 are even more impressive.

3. MATHEMATICAL MODEL FOR MIMO GMTI OBSERVATIONS

In this section is developed a mathematical model related to that utilized in [15], but modified to highlight the issue of the clutter rank. The simple linear antenna array layout shown in Figure 3.1 is utilized. The T transmitters are equally spaced by ($\lambda/2$). The R receivers are spaced by (T $\lambda/2$), resulting in a critical ($\lambda/2$) spacing for the virtual array of RT elements. The leftmost antenna is used as a transmit/receive element and is the phase center used for the mathematical modeling. The platform is assumed to travel in a direction parallel with the array axis, for simplicity. Figure 3.1 illustrates the case of (T = 3, R = 4), but the analysis is performed for arbitrary values of T and R, and holds equally if the receivers were made closer together and the transmitters farther apart. To focus on the clutter rank issue, the analysis is performed by including just the clutter on the ray that is isoDoppler to the target (see Section 2). As noted in the Introduction, the analysis treats only the cases in which there is exactly one such ray. If that clutter is at off-broadside angle θ (the off-broadside angle is the complement of the cone angle), then any point on the clutter ray will observe (in the far field) a phase between adjacent transmitters of

$$\phi = 2\pi\left(\lambda/2\right)\sin\theta/\lambda = \pi\sin\theta, \tag{3.1}$$

due to the $\lambda/2$ spacing of transmitters. Because high-speed targets may not have isoDoppler clutter on the ground, the analytical results herein are simpler to state in terms of ϕ rather than the target velocity.

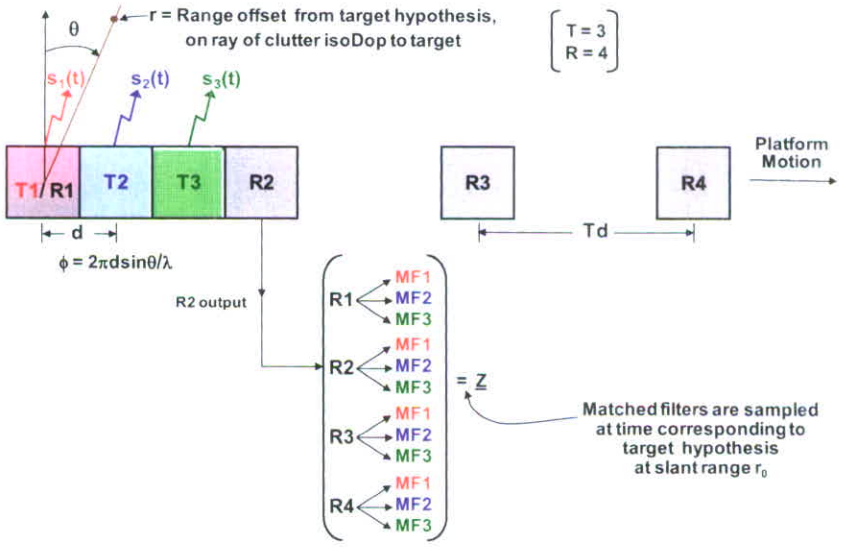

Figure 3.1. MIMO transmission and reception.

The transmitted waveforms are designated as $\{s_1(t),\ldots,s_T(t)\}$, in analytical signal notation [20, pp. 57–60]. If the hypothesized target is at (slant) range r_0 from the platform, the waveforms would superpose at that range on the clutter ray proportional to the scalar time function

$$\sum_{i=1}^{T} s_i\left(t - r_0 / c\right) e^{j(i-1)\phi}, \tag{3.2}$$

where the phasors represent the transmitter phase offsets on the clutter ray[5]. For a clutter patch on the ray displaced from the target range by r, the superposition in (3.2) would become instead

$$\sum_{i=1}^{T} s_i\left(t - \left[r_0 + r\right] / c\right) e^{j(i-1)\phi}. \tag{3.3}$$

If this patch has complex reflectivity q(r) (including 2-way r-dependent propagation loss and antenna gain), then at the phase-reference antenna (i.e., antenna #1) the reception would be proportional to

$$\sum_{i=1}^{T} s_i\left(t - 2\left[r_0 + r\right] / c\right) e^{j(i-1)\phi} q\left(r\right), \tag{3.4}$$

because of this patch of clutter. The superposition of all the clutter patches on the ray would be observed as

$$\sum_{r}\sum_{i=1}^{T} s_i\left(t - 2\left[r_0 + r\right] / c\right) e^{j(i-1)\phi} q\left(r\right). \tag{3.5}$$

As discussed in Section 2, the focus here is on the case of an extended range domain of clutter, where the clutter ray extends on both sides of the hypothesized target range, to a distance beyond that corresponding to the finite coherent processing interval of the radar. This makes the sum over (r) in (3.5) effectively cover an infinite extent of range, both positively and negatively. The matched filter for the k^{th} waveform, at the output of this antenna is now considered. When that matched filter is sampled at a time of $(2r_0/c)$,

---

[5] The expression in (3.2) is valid when the waveforms $\{s_i(t)\}$ represent the various transmissions over the full coherent processing interval. For repetitive, pulsed-Doppler radar, it is convenient to think of the $\{s_i(t)\}$ as being just the pulse waveforms. For that interpretation, (3.2) should include range ambiguities. However, in the assumed geometry the range ambiguities for a given Doppler frequency are at the same angle-of-arrival. Thus, while the ambiguities contribute added clutter power, they do not change the functional form of the MIMO clutter covariance. Thus, (3.2) can serve for both cases.

corresponding to the hypothesized target range, it effectively correlates its input function with $s_k(t - 2r_0/c)$ [17, p. 153]. For the clutter input in (3.5), the output of the matched filter would be

$$\begin{aligned} z_k &= \int s_k^*\left(t-2r_0/c\right)\left[\sum_r\sum_{i=1}^{T} s_i\left(t-2\left[r_0+r\right]/c\right)e^{j(i-1)\phi}q\left(r\right)\right]dt. \\ &= \sum_r\sum_{i=1}^{T}\left[\int s_k^*\left(t-2r_0/c\right)s_i\left(t-2\left[r_0+r\right]/c\right)dt\right]e^{j(i-1)\phi}q\left(r\right) \\ &= \sum_r\sum_{i=1}^{T} c_{ki}\left(-2r/c\right)e^{j(i-1)\phi}q\left(r\right), \end{aligned} \tag{3.6}$$

where $c_{ki}(\cdot)$ is the cross-correlation between the kth and ith waveforms, defined by

$$c_{ki}\left(\gamma\right) = \int s_k^*\left(t\right)s_i\left(t+\gamma\right)dt. \tag{3.7}$$

Equation (3.6) can be rewritten as

$$z_k = \sum_r \left[c_{k1}\left(-2r/c\right),\ldots,c_{kT}\left(-2r/c\right)\right]\underline{v}_T\left(\phi\right)q\left(r\right), \tag{3.8}$$

where $\underline{v}_T(\phi)$ is the Vandermonde vector of the transmitter phase offsets on the clutter ray:

$$\underline{v}_T\left(\phi\right) \triangleq \left[1, e^{j\phi},\ldots,e^{j(T-1)\phi}\right]^T. \tag{3.9}$$

Thus, coming from the T matched filters following antenna #1, the following vector is obtained:

$$\begin{pmatrix} z_1 \\ \vdots \\ z_T \end{pmatrix} = \sum_r C\left(-2r/c\right)\underline{v}_T\left(\phi\right)q\left(r\right), \tag{3.10}$$

where $C(\cdot)$ is the matrix of waveform cross-correlations:

$$\left[C(\tau)\right]_{k,i} = c_{ki}\left(\tau\right). \tag{3.11}$$

The receivers are spaced apart by (Tλ/2); hence the outputs of the T matched filters following the k^{th} receiver are the same as the vector (3.10), multiplied by the scalar phasor exp[j(k − 1)Tϕ]. When the T-vector outputs of the R receivers are stacked as shown in Figure 3.1, one obtains the RT-vector—the R = 4, T = 3 case is examined first, to make a point after (3.14):

$$\underline{z} = \begin{bmatrix} 1 & 0 & 0 \\ 0 & 1 & 0 \\ 0 & 0 & 1 \\ e^{j3\phi} & 0 & 0 \\ 0 & e^{j3\phi} & 0 \\ 0 & 0 & e^{j3\phi} \\ & \vdots & \\ e^{j9\phi} & 0 & 0 \\ 0 & e^{j9\phi} & 0 \\ 0 & 0 & e^{j9\phi} \end{bmatrix} \sum_r C\left(-2r/c\right) \underline{v}_T(\phi) q(r). \tag{3.12}$$

For general R and T, (3.12) becomes

$$\underline{z} = \left[\underline{v}_R(\phi) \otimes I_T\right] \sum_r C(-2r/c) \underline{v}_T(\phi) q(r), \tag{3.13}$$

where

$$\underline{v}_R(\phi) \triangleq \begin{bmatrix} 1 \\ e^{j\phi T} \\ \vdots \\ e^{j(R-1)\phi T} \end{bmatrix}, \tag{3.14}$$

and ⊗ denotes a Kronecker product [21, p. 21]. It is observed that the (12 × 3) matrix on the right-hand side (RHS) of (3.12) has three orthogonal columns, for T = 3. This warns of the possibility of a rank-T covariance for $\underline{z}$, as will be encountered below, when the waveforms are uncorrelated.

As an important aside, it is useful to use (3.13) to derive the MIMO response to a hypothesized point target. The target would be at r = 0. For equal-power waveforms uncorrelated at 0 delay, C(0) becomes $c_{11}(0)\, I_T$. Then (3.13) becomes, for the target,

$$\begin{aligned} \underline{z}_t &= \left[\underline{v}_R(\phi_t) \otimes I_T\right] c_{11}(0)\, \underline{v}_T(\phi_t)\, q_t \\ &= \left[1, e^{j\phi_t}, \ldots, e^{j(RT-1)\phi_t}\right]^T c_{11}(0)\, q_t, \end{aligned} \tag{3.15}$$

where ϕ_t is the phase between transmitters at the target, and q_t is the complex reflectivity of the target. The Vandermonde vector in (3.15) is the convolution of the receiver and transmitter locations, which is referred to as the MIMO virtual array [1, 3, 8]. Other values for C(0) would give other responses in (3.15), but always a single steering vector for the target. The fact that the clutter is extended in range forces the use of (3.13), with its multiple steering vectors, in place of (3.15) for a point source. The impact will be seen below.

The clutter patches are typically modeled as having independent reflectivities. As the patches shrink, (3.13) is replaced by the integral

$$\underline{z} = \left[\underline{v}_R(\phi) \otimes I_T\right] \int C(-2r/c)\, \underline{v}_T(\phi)\, q(r)\, dr, \tag{3.16}$$

where q(r) is a complex, circular Gaussian white-noise random process [22, pp. 65–72], corresponding to the "sandpaper earth" approximation for clutter, which is held to be valid when the granularity of the clutter is coarser than the wavelength of the radar. Changing variables in (3.16), one obtains

$$\underline{z} = \left[\underline{v}_R(\phi) \otimes I_T\right] \int C(\tau)\, \underline{v}_T(\phi)\, q(-c\tau/2)\, d\tau,$$

and because $q(-c\tau/2)$ is still a white noise (having a scaled power spectral density), it is renamed $u(\tau)$ for ease:

$$\underline{z} = \left[\underline{v}_R(\phi) \otimes I_T\right] \int C(\tau)\, \underline{v}_T(\phi)\, u(\tau)\, d\tau. \tag{3.17}$$

Because the columns of the first matrix on the RHS of (3.17) are orthogonal, it will be observed that it's the variation of the T × T matrix $C(\tau)$ over τ that is critical. This variation is constrained by the fact that $C(\tau)$ is the cross-correlation between actual waveforms, resulting in the findings that were outlined in Section 1.

Continuing the modeling, the correlation function of u(τ) is written as

$$E\left[u(\tau)u^*(\tau_1)\right] = p(\tau)\delta(\tau-\tau_1), \tag{3.18}$$

where $\delta(\cdot)$ is the Dirac delta function. The function $p(\tau)$ includes the impact of variability of antenna gains, terrain cover, and propagation losses. For simplicity, $p(\tau)$ will be set to unity in this analysis. To simplify the notation, one can define the following:

$$B(\phi) \triangleq \left[\underline{v}_R(\phi) \otimes I_T\right]. \tag{3.19}$$

It is observed that $\left[B(\phi)\left(1/\sqrt{R}\right)\right]$ is an orthonormal set of T vectors, each having dimension RT. The covariance of $\underline{z}$ from clutter on the isoDop ray has been referred to as the MIMO virtual covariance matrix associated with the target Doppler bin [3]. For brevity, it is referred to here as the MIMO clutter covariance. From (3.17–19), it can be written as

$$\begin{aligned}\Sigma(\phi) \triangleq E\left[\underline{z}\underline{z}^H\right] &= B(\phi)\left[\iint C(\tau)\underline{v}_T(\phi)\delta(\tau-\tau_1)\underline{v}_T^H(\phi)C^H(\tau_1)d\tau d\tau_1\right]B^H(\phi) \\ &= B(\phi)H(\phi)B^H(\phi),\end{aligned} \tag{3.20}$$

where the sifting property of the Dirac delta function has been used, and the resulting integral has been abbreviated by

$$H(\phi) \triangleq \int G(\tau,\phi)d\tau, \tag{3.21}$$

where

$$G(\tau,\phi) \triangleq C(\tau)\underline{v}_T(\phi)\underline{v}_T^H(\phi)C^H(\tau). \tag{3.22}$$

Because $G(\tau,\phi)$ is (T × T), positive-semidefinite Hermitian for all (τ,ϕ), $H(\phi)$ is also (T × T), positive-semidefinite Hermitian. Thus, one can write an eigendecomposition for $H(\phi)$ as

$$H(\phi) = F(\phi)\Lambda(\phi)F^H(\phi), \tag{3.23}$$

where $\Lambda(\phi)$ is diagonal, non-negative real. Because $\left[B(\phi)\left(1/\sqrt{R}\right)\right]$ has orthonormal columns, one can use (3.23) to write the eigendecomposition of $\Sigma(\phi)$ as

$$\Sigma(\phi)=\left[B(\phi)F(\phi)\left(1/\sqrt{R}\right)\right]\left[\Lambda(\phi)R\right]\left[B(\phi)F(\phi)\left(1/\sqrt{R}\right)\right]^{H}, \tag{3.24}$$

where it is clear that the columns of the first factor in brackets on the RHS are orthonormal. Thus, $\Sigma(\phi)$ has (RT – T) eigenvalues of zero, and T eigenvalues scaled up from those of $H(\phi)$ (some of which may also be zero):

$$\lambda_i\left(\Sigma(\phi)\right)=\left\{\begin{matrix} R\cdot\lambda_i\left(H(\phi)\right) & ;(i=1,\ldots,T), \\ 0 & ;(i=T+1,\ldots,RT) \end{matrix}\right\}. \tag{3.25}$$

The eigenvalues are considered to be written in descending order.

Some mathematical preliminaries are now covered. First, as is well known, the cross-correlation functions satisfy

$$\begin{aligned} c_{k\ell}(\tau) &= \int s_k^*(t)\,s_\ell(t+\tau)\,dt \\ &= \int\left[\int S_k(f)e^{j2\pi ft}df\right]^*\left[\int S_\ell(\gamma)e^{j2\pi\gamma(t+\tau)}d\gamma\right]dt \\ &= \iint S_k^*(f)S_\ell(\gamma)e^{j2\pi\gamma\tau}\left[\int e^{-j2\pi(f-\gamma)t}dt\right]d\gamma df \\ &= \iint S_k^*(f)S_\ell(\gamma)e^{j2\pi\gamma\tau}\delta(f-\gamma)\,d\gamma df \\ &= \int S_k^*(f)S_\ell(f)e^{j2\pi f\tau}df, \end{aligned} \tag{3.26}$$

where $S_k(f)$ represents the Fourier transform of $s_k(t)$. Thus, $S_k^*(f)S_\ell(f)$ is the Fourier transform of $c_{k\ell}(\tau)$:

$$F\left[c_{k\ell}(\tau)\right]=S_k^*(f)S_\ell(f). \tag{3.27}$$

Because of the expressions in (3.21–22), there is particular interest in integrals of the form

$$\begin{aligned}\int\left[c_{ij}(\tau)c_{k\ell}^{*}(\tau)\right]d\tau &= \int\left[\int S_i^{*}(f)S_j(f)e^{j2\pi f\tau}df\right]\left[\int S_k^{*}(\gamma)S_\ell(\gamma)e^{j2\pi\gamma\tau}d\gamma\right]^{*}d\tau \\ &= \iint S_i^{*}(f)S_j(f)S_k(\gamma)S_\ell^{*}(\gamma)\left[\int e^{j2\pi(f-\gamma)\tau}d\tau\right]d\gamma df \\ &= \iint S_i^{*}(f)S_j(f)S_k(\gamma)S_\ell^{*}(\gamma)\delta(f-\gamma)d\gamma df \\ &= \int S_i^{*}(f)S_j(f)S_k(f)S_\ell^{*}(f)df \qquad (3.28)\end{aligned}$$

$$\triangleq \Phi_{ijk\ell}. \qquad (3.29)$$

Due to (3.29), there are many symmetries between the indices of $\Phi_{ijk\ell}$, for example,

$$\Phi_{ijk\ell} = \Phi_{\ell kji} = \Phi_{k\ell ij}^{*}. \qquad (3.30)$$

Integrals of the form (3.29) are inviting for the application of Schwarz's inequality, which will be utilized in Section 5. In the past, the Schwartz inequality has been used on quantities like those in (3.28), to develop various bounds related to correlation properties of discrete sequences [23, 24].

It is assumed herein that

$$c_{\ell\ell}(0) > 0; (\ell = 1,...,T). \qquad (3.31)$$

Combining this with (3.29) yields

$$\Phi_{\ell\ell\ell\ell} = \int |c_{\ell\ell}(\tau)|^2 \, d\tau > 0; (\ell = 1,...,T). \qquad (3.32)$$

It previously had been pointed out by Keith Forsythe of Lincoln Laboratory that ideal waveform sets cannot in fact exist over extended domains of range, where an ideal waveform set would consist of waveforms that are pairwise uncorrelated for all delays but have identical autocorrelation functions [19]. Using the tools above, one easily can see why such sets cannot exist. If $s_k(t)$ and $s_\ell(t)$ are uncorrelated at all delays, then

$$\int |c_{k\ell}(\tau)|^2 \, d\tau = 0. \qquad (3.33)$$

But then, by (3.29),

$$\Phi_{k\ell k\ell} = 0. \tag{3.34}$$

In particular, from (3.29),

$$\int |S_k(f)|^2 |S_\ell(f)|^2 \, df = 0, \tag{3.35}$$

$$\Phi_{\ell\ell kk} = 0. \tag{3.36}$$

So $S_k(f)$ and $S_\ell(f)$ share no frequency support. Now, one can examine the mismatch between the autocorrelation functions $c_{kk}(\tau)$ and $c_{\ell\ell}(\tau)$. To do this, one can use the generalized cosine between two functions of τ:

$$\cos^2(\kappa) \triangleq \frac{\left|\int c_{kk}^*(\tau) c_{\ell\ell}(\tau) d\tau\right|^2}{\left[\int |c_{kk}(\tau)|^2 \, d\tau\right]\left[\int |c_{\ell\ell}(\tau)|^2 \, d\tau\right]}$$

$$= |\Phi_{\ell\ell kk}|^2 / \left[\Phi_{kkkk}\Phi_{\ell\ell\ell\ell}\right]$$
$$= 0, \tag{3.37}$$

where the last step follows from (3.36). Thus, $c_{kk}(\tau)$ and $c_{\ell\ell}(\tau)$ are orthogonal (hence maximally mismatched). From the discussion in Section 1 of the matched-filter weightings of the ground clutter on the isoDopppler ray, the drastic mismatch of autocorrelation functions for the different waveforms of the set, combined with zero cross-correlation, is expected to cause decorrelations in the clutter covariance matrix. That will be quantified in Section 4.

It is noted here that if all the waveforms are proportional (i.e., SIMO), then (3.7, 11) imply that

$$s_i(t) = d_i s(t); (i = 1, \ldots, T),$$
$$C(\tau) = \underline{d} c(\tau) \underline{d}^H, \ for \ \underline{d} \in \mathbb{C}^T, \tag{3.38}$$

where $c(\tau)$ is the autocorrelation function of s(t). Then in (3.22)

$$\begin{aligned} G(\tau,\phi) &= \underline{d}\; c(\tau)\underline{d}^H \underline{v}_T(\phi)\underline{v}_T^H(\phi)\underline{d}c^*(\tau)\underline{d}^H \\ &= \underline{d}\;|c(\tau)\underline{d}^H \underline{v}_T(\phi)|^2\;\underline{d}^H, \end{aligned} \tag{3.39}$$

which has at most one nonzero eigenvalue, whose only potential eigenvector $(\underline{d})$ is constant in direction over the domain of τ. Thus, $H(\phi)$, in (3.21) has rank 0 or 1. In fact, if waveforms could be designed to be dependent on the hypothesized value of ϕ, it would be possible to make $H(\phi)$ have rank 0—by choosing $\underline{d}$ in (3.39) to be perpendicular to $\underline{v}_T(\phi)$—making $\Sigma(\phi)$ also be of rank 0, by (3.25). This is just transmit nulling of the clutter ray. In this work, it is assumed that a single set of waveforms is employed for all hypothesized values of ϕ, which rules out that possibility. Note that (3.38) is just a special case of delay similarity of the waveform cross-correlation matrix (Condition C of Figure 6.1), which always guarantees that $H(\phi)$ has rank 1 or 0.

Returning to the mathematical preliminaries, from (3.9, 11, 22) one obtains

$$G(\tau,\phi) = \begin{bmatrix} \sum_{i=1}^{T} c_{1i}(\tau)e^{j\phi(i-1)} \\ \vdots \\ \sum_{i=1}^{T} c_{Ti}(\tau)e^{j\phi(i-1)} \end{bmatrix} \begin{bmatrix} \sum_{i=1}^{T} c_{1i}(\tau)e^{j\phi(i-1)} \\ \vdots \\ \sum_{i=1}^{T} c_{Ti}(\tau)e^{j\phi(i-1)} \end{bmatrix}^H \tag{3.40}$$

$$\left[G(\tau,\phi)\right]_{mn} = \sum_{k=1}^{T}\sum_{i=1}^{T} c_{mi}(\tau)c_{nk}^*(\tau)e^{j\phi(i-k)}. \tag{3.41}$$

Hence, from (3.21, 29)

$$\left[H(\phi)\right]_{m,n} = \sum_{k=1}^{T}\sum_{i=1}^{T} e^{j\phi(i-k)}\Phi_{mink}. \tag{3.42}$$

Equation (3.42) will be used in the next section.

4. MIMO CLUTTER COVARIANCE FOR UNCORRELATED WAVEFORMS

When the waveforms are pairwise uncorrelated, equations (3.33–36) hold for any pair of waveforms from the set. Thus, for (3.42),

$$\Phi_{mink} = 0, \; unless \; m = i = n = k. \tag{4.1}$$

But then, from (3.42),

$$\left[H(\phi) \right]_{m,n} = \left\{ \begin{matrix} T\Phi_{mmmm} \; ; & (m = n) \\ 0 \quad ; & otherwise \end{matrix} \right\}; (\forall \phi). \tag{4.2}$$

If one merely assumes that in (3.32)

$$\Phi_{mmmm} = \Phi; (\forall m), \tag{4.3}$$

then

$$H(\phi) = T\Phi I_T; (\forall \phi), \tag{4.4}$$

having T equal eigenvalues. However, recall from (3.25) that the nonzero eigenvalues of $\Sigma(\phi)$, the MIMO clutter covariance, are just scaled up from those of $H(\phi)$. Thus, $\Sigma(\phi)$ also has T equal, positive eigenvalues, a poor situation for clutter cancellation. Note that this is true for all values of ϕ.

The result in (4.4) also allows one to see why the SINR loss curve as a function of velocity has different shapes, depending on whether the transmitters or receivers are spaced far apart physically. For uncorrelated waveforms, (4.4) says that $H(\phi)$ is a scaled identity matrix. But any set of weights, $\underline{w}$, that fully cancels the clutter must satisfy

$$\begin{aligned} E\left[\| \underline{w}^H \underline{z} \|^2 \right] &= 0 \\ \underline{w}^H \Sigma(\phi) \underline{w} &= 0. \end{aligned} \tag{4.5}$$

So, using (3.20) and (4.4), the weights must satisfy

$$\underline{w}^H B(\phi) T\Phi I_T B^H(\phi)\underline{w} = 0.$$
$$T\Phi \,\|\, B^H(\phi)\underline{w}\|^2 = 0. \tag{4.6}$$

Thus, $\underline{w}$ must be orthogonal to each column of $B(\phi)$, as exemplified by the first factor on the RHS of (3.12), and written out in (3.19). However, these columns have no common elements between transmitters, relying instead on just the receiver outputs for a single transmitter to cancel one another. Thus, when the receivers are close together, the SINR notch is wide due to poor angular resolution, as shown in Figure 1.6. When the receivers are spaced at greater-than-critical spacing, there are multiple thin notches in the SINR loss curve because of ambiguities in the receiver array response. The computer simulation results for this case are shown in Figure 4.1[6]. The fact that the receive array alone is responsible for clutter cancellation when the waveforms are uncorrelated makes MIMO perform like SIMO in this respect.

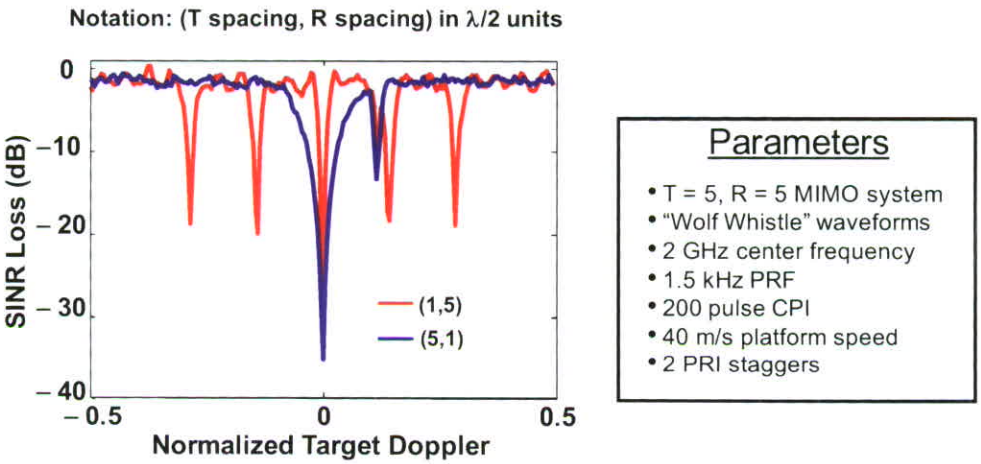

Figure 4.1. The blue curve repeats results from Figure 1.6, with closely spaced receivers. The red curve is for widely spaced receivers, causing array ambiguities.

---

[6] Recall from the discussion of Figure 1.6 that there was an extra target in the training data, causing extra SINR loss at a hypothesized normalized target Doppler of about 0.1. That extra loss affects both array layouts in Figure 4.1, due to the use of realistic, low-correlation waveforms, which require extra degrees of freedom to attempt to cancel the isoDop clutter ray together with the direction of the true target in the training data.

5. IMPACT OF UNEQUAL WAVEFORMS ON THE SECOND EIGENVALUE OF THE MIMO CLUTTER COVARIANCE, WHEN T = 2

In this section, it shall be seen that when T = 2 there is a quadratic penalty on the product of the highest two eigenvalues of the MIMO clutter covariance when the two waveforms are not proportional. This yields information about the behavior of the second eigenvalue.

One starts by writing out (3.22), using (3.9, 11);

$$G(\tau,\phi)=\begin{bmatrix} c_{11}(\tau)c_{11}^{*}(\tau)+c_{11}c_{12}^{*}e^{-j\phi} & c_{11}c_{21}^{*}+c_{11}c_{22}^{*}e^{-j\phi} \\ +c_{12}e^{j\phi}c_{11}^{*}+c_{12}c_{12}^{*}(\tau) & +c_{12}e^{j\phi}c_{21}^{*}+c_{12}c_{22}^{*}(\tau) \\ c_{21}c_{11}^{*}+c_{21}c_{12}^{*}e^{-j\phi} & c_{21}c_{21}^{*}+c_{21}c_{22}^{*}e^{-j\phi} \\ +c_{22}e^{j\phi}c_{11}^{*}+c_{22}c_{12}^{*}(\tau) & +c_{22}e^{j\phi}c_{21}^{*}+c_{22}c_{22}^{*}(\tau) \end{bmatrix}, \tag{5.1}$$

where the argument (τ) has been left off of most of the $c_{ij}(\tau)$, for brevity. As indicated in (3.21), one must integrate $G(\tau,\phi)$ over τ to obtain $H(\phi)$. Using (3.29), one obtains:

$$H(\phi)=\begin{bmatrix} \Phi_{1111}+\Phi_{1112}e^{-j\phi} & \Phi_{1121}+\Phi_{1122}e^{-j\phi} \\ +\Phi_{1211}e^{j\phi}+\Phi_{1212} & +\Phi_{1221}e^{j\phi}+\Phi_{1222} \\ & \\ \Phi_{2111}+\Phi_{2112}e^{-j\phi} & \Phi_{2121}+\Phi_{2122}e^{-j\phi} \\ +\Phi_{2211}e^{j\phi}+\Phi_{2212} & \Phi_{2221}e^{j\phi}+\Phi_{2222} \end{bmatrix}. \tag{5.2}$$

Recall from Section 3 that $G(\tau,\phi)$ and $H(\phi)$ are both positive-semidefinite Hermitian matrices. Thus, the second eigenvalue of $H(\phi)$ is never negative, and is positive iff the determinant of $H(\phi)$ is positive. The mathematical expression for the determinant is simpler than that for the second eigenvalue, so only the determinant is studied here. Because many of the exponentials in the determinant integrate to 0, one examines the following expression, instead of studying various values of ϕ individually:

$$\underset{\phi}{Average}\left\{\det\left[H(\phi)\right]\right\}. \tag{5.3}$$

When the quantity in (5.3) is positive, then $\lambda_{\min}\left[H(\phi)\right]$ cannot be 0 for all ϕ, and so $\lambda_2\left[\Sigma(\phi)\right]$ in (3.25) cannot be 0 for all ϕ; thus, $\Sigma(\phi)$ (the MIMO clutter covariance) cannot have rank 1 or 0 for all ϕ. A quadratic penalty on (5.3) will be derived, which applies when the waveforms are not proportional.

Continuing the analysis, one recalls that

$$\det\begin{bmatrix} w_{11} & w_{12} \\ w_{21} & w_{22} \end{bmatrix} = w_{11}w_{22} - w_{12}w_{21}. \tag{5.4}$$

If one applies this to (5.2) and averages over ϕ, (5.3) becomes

$$\begin{aligned} Average\left\{\det\left[H(\phi)\right]\right\} = {} & \Phi_{1111}\Phi_{2121} + \Phi_{1111}\Phi_{2222} + \Phi_{1212}\Phi_{2222} \\ & -\left(\Phi_{2111}\Phi_{1121} + \Phi_{2112}\Phi_{1221} + \Phi_{2212}\Phi_{1222}\right). \end{aligned} \tag{5.5}$$

To derive this expression, some simple symmetries similar to (3.30) have been used. The Schwarz inequality will be employed (multiple times) on the RHS of (5.5). The version employed includes a remainder term, and is equivalent to the Pythagorean theorem, which is now discussed.

The Pythagorean theorem is now examined, as applied to the L_2 space of square-integrable, complex functions (see [25, pp. 49–52]). Its relation to the Schwarz inequality will also be brought out. In Figure 5.1, a(f) and b(f) are complex functions of the continuous variable (f). In the analysis herein, (f) represents frequency. Different values of (f) can be considered as the coordinates, with a(f) and b(f) being infinite-dimensional vectors on these coordinates, in the vector space of L_2. The dot product in this vector space is analogous to that of finite-dimensional vectors:

$$\langle a,b\rangle \triangleq \int b^*(f)a(f)df, \tag{5.6}$$

and

$$\| b \|^2 \triangleq \langle b,b\rangle = \int |b(f)|^2 df \geq 0, \tag{5.7}$$

with equality iff $b(\cdot)$ is the 0 function (sets of measure 0 can be ignored, because it would take waveforms of infinite duration to generate a Dirac delta function in the frequency domain). Define, when (b) is of nonzero norm,

$$P_b a \triangleq \frac{b(f)\langle a,b\rangle}{\| b \|^2}. \tag{5.8}$$

This quantity is called the projection of (a) onto (b), because P_ba is parallel to (b)—obvious from (5.8)—and the residual error

$$e(f) \triangleq a(f) - P_b a \tag{5.9}$$

is perpendicular to (b) (and hence is also perpendicular to P_ba):

$$\begin{aligned}
\langle e,b\rangle &= \int \left[a(f) - P_b a(f)\right]\left[b^*(f)\right] df \\
&= \int \left[a(f) - \frac{\langle a,b\rangle}{\|b\|^2} b(f)\right]\left[b^*(f)\right] df \\
&= \langle a,b\rangle - \frac{\langle a,b\rangle \|b\|^2}{\|b\|^2} \\
&= 0.
\end{aligned} \tag{5.10}$$

Thus, Figure 5.1 shows a right angle between (e) and (b). From (5.9), one may write a(f) as

$$a(f) = e(f) + P_b a, \tag{5.11}$$

where the two terms on the RHS are orthogonal. Taking the norm^2 of (5.11) and using the fact that (e) is perpendicular to P_ba, one obtains (cross terms are 0)

$$\|a\|^2 = \|e\|^2 + \|P_b a\|^2, \tag{5.12}$$

which is the Pythagorean theorem, for this right triangle in function space.

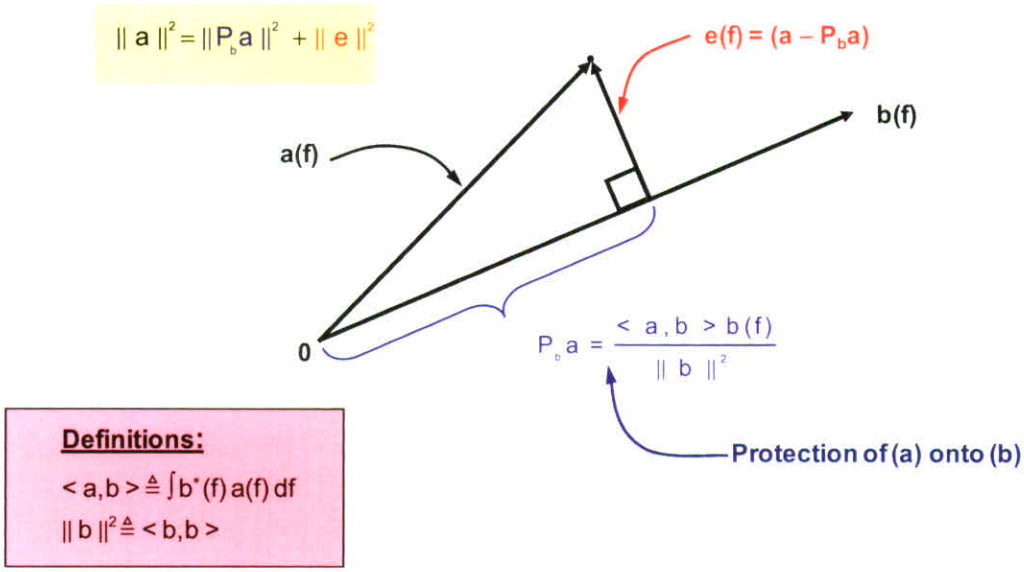

Figure 5.1. Pythagorean theorem in L_2 function space.

As a brief aside, note that the Schwarz inequality merely recognizes that $\left[\|e\|^2 \geq 0\right]$ in (5.12), to say that

$$\begin{aligned} \|a\|^2 &\geq \|P_b a\|^2 \\ &= \int \left| \frac{\langle a,b \rangle}{\|b\|^2} b(f) \right|^2 df \\ &= \frac{|\langle a,b \rangle|^2}{\|b\|^2}, \end{aligned} \tag{5.13}$$

so that one has

$$\|a\|^2 \|b\|^2 \geq |< a,b >|^2, \tag{5.14}$$

with equality iff [e = 0]—i.e., when (a) is parallel to (b).

For application here, transpose (5.12) to obtain

$$\|a\|^2 - \|P_b a\|^2 = \|e\|^2, \tag{5.15}$$

which can be written out as

$$\int |a(f)|^2 df - \frac{|\langle a,b\rangle|^2}{\|b\|^4}\int |b(f)|^2 df = \int \left| a(f) - \frac{\langle a,b\rangle}{\|b\|^2} b(f)\right|^2 df,$$

$$\left[\int |b(f)|^2\, df\right]\left[\int |a(f)|^2\, df\right] - \left|\int a(f)b^*(f)df\right|^2 = \|b\|^2 \int \left| a(f) - \frac{\langle a,b\rangle}{\|b\|^2} b(f)\right|^2 df\,. \tag{5.16}$$

The term on the RHS of (5.16) is ($\geq$0), with equality iff:

$$a(f) = \gamma b(f); (\forall f), \textit{for some}\ \gamma\,. \tag{5.17}$$

(Recall that sets of measure 0 are ignored here.)

One may now apply (5.16) to (5.5), multiple times. Studying the form of (5.5), one finds six terms on the RHS, each being a product of two Φ factors. To write subsets of terms from the RHS of (5.5) in the form of the LHS of (5.16), one should use two terms per subset. One needs to choose the correct three pairs of terms, and to choose a(f) and b(f) appropriately for each pair. Hypothesize that a(f) and b(f) both consist of products of $S_1(f)$ and $S_2(f)$, and their conjugates. Note from the LHS of (5.16) that in both terms there are second-order products both in a(f) and in b(f). The hypothesis then forces one to group terms from the RHS of (5.5) having identical total counts of indices 1 and 2. This yields the following grouping:

$$\begin{aligned}\underset{\phi}{Avg.}\left\{\det\left[H(\phi)\right]\right\} = &\left[\Phi_{1111}\Phi_{2121} - \Phi_{2111}\Phi_{1121}\right] \\ &+ \left[\Phi_{1111}\Phi_{2222} - \Phi_{2112}\Phi_{1221}\right] \\ &+ \left[\Phi_{1212}\Phi_{2222} - \Phi_{2212}\Phi_{1222}\right] \\ &\triangleq \Delta_1 + \Delta_2 + \Delta_3.\end{aligned} \tag{5.18}$$

One still must identify a(f) and b(f) for each bracketed term. Recall from (5.8) that (b) must have positive norm. One arrives at the following identifications, which end up working out well, as will be seen.

First term on RHS of (5.18)

$$b(f) = S_1^*(f) S_1(f);\ a(f) = S_2^*(f) S_1(f). \tag{5.19}$$

From (3.29, 5.18, 5.19) and the RHS of (5.16),

$$\begin{aligned} \Delta_1 &= \|b\|^2 \int \left| a(f) - \frac{\langle a,b \rangle}{\|b\|^2} b(f) \right|^2 df \\ &= \left[\int |S_1(f)|^4 \, df \right] \left[\int \left| S_2^*(f) S_1(f) - \frac{< S_2^* S_1, |S_1|^2 >}{\| |S_1|^2 \|^2} |S_1(f)|^2 \right|^2 df \right]. \end{aligned} \tag{5.20}$$

One obtains from (5.17) that $(\Delta_1 \geq 0)$, and

$$\begin{aligned} &\Delta_1 = 0 \ \textit{iff}\ S_2^*(f) S_1(f) = \gamma_1 S_1^*(f) S_1(f); (\forall f), (V\gamma_1) \\ &\left[S_2^*(f) - \gamma_1 S_1^*(f) \right] S_1(f) = 0 \\ &S_2(f) = \gamma_1^* S_1(f); \textit{whenever}\ S_1(f) \neq 0, (V\gamma_1). \end{aligned} \tag{5.21}$$

Second term on RHS of (5.18)

$$b(f) = S_1^2(f); a(f) = S_2^2(f). \tag{5.22}$$

From (5.18, 19) and the RHS of (5.16) (as above),

$$\Delta_2 = \left[\int |S_1(f)|^4 df\right]\left[\int \left| S_2^2(f) - \frac{\langle S_2^2, S_1^2\rangle}{\|S_1^2\|^2} S_1^2(f)\right|^2 df\right]. \tag{5.23}$$

One obtains from (5.17) that $(\Delta_2 \geq 0)$, and

$$\Delta_2 = 0 \text{ iff } S_2^2(f) = \gamma_2 S_1^2(f); (\forall f), (V\gamma_2). \tag{5.24}$$

Third term on RHS of (5.18)

$$b(f) = S_2(f) S_2^*(f); a(f) = S_1^*(f) S_2(f). \tag{5.25}$$

Analogously to above is

$$\Delta_3 = \left[\int |S_2(f)|^4 df\right]\left[\int \left| S_1^*(f) S_2(f) - \frac{\langle S_1^* S_2, |S_2|^2\rangle}{\|\,|S_2|^2\|^2} |S_2(f)|^2\right|^2 df\right]. \tag{5.26}$$

From (5.17), $(\Delta_3 \geq 0)$, and

$$\begin{aligned} &\Delta_3 = 0 \text{ iff } S_1^*(f) S_2(f) = \gamma_3 S_2(f) S_2^*(f); (\forall f), (V\gamma_3), \\ &\left[S_1^*(f) - \gamma_3 S_2^*(f)\right] S_2(f) = 0 \\ &\qquad S_1(f) = \gamma_3^* S_2(f); \textit{whenever } S_2(f) \neq 0, (V\gamma_3). \end{aligned} \tag{5.27}$$

From (5.18, 21, 24, 27), one concludes that

$$\underset{\phi}{Avg.}\left\{\det\left[H(\phi)\right]\right\} = \Delta_1 + \Delta_2 + \Delta_3 \geq 0, \tag{5.28}$$

with equality iff

$$S_2(f) = \gamma S_1(f); (\forall f), (V\gamma). \tag{5.29}$$

One simple way to obtain (5.29) is to observe that (5.24) shows that $S_1(f)$ and $S_2(f)$ must have identical nonzero supports, and then (5.21, 27) easily lead to (5.29).

Now, one may apply (5.28) to (3.25), to reach conclusions for the MIMO clutter covariance. First, recall that

$$\underset{\phi}{Avg.}\left\{\det\left[H(\phi)\right]\right\} = \underset{\phi}{Avg.}\left\{\prod_{i=1}^{T} \lambda_i\left[H(\phi)\right]\right\} \tag{5.30}$$

$$= \underset{\phi}{Avg.}\left\{\lambda_1\left[H(\phi)\right]\lambda_2\left[H(\phi)\right]\right\}, \tag{5.31}$$

because T = 2 in this section. But then, from (3.25), (5.28, 31),

$$\begin{aligned} \underset{\phi}{Avg.}\left\{\lambda_1\left[\Sigma(\phi)\right]\lambda_2\left[\Sigma(\phi)\right]\right\} &= R^2 \underset{\phi}{Avg.}\left\{\lambda_1\left[H(\phi)\right]\lambda_2\left[H(\phi)\right]\right\} \\ &= R^2 \underset{\phi}{Avg.}\left\{\det\left[H(\phi)\right]\right\} \\ &= R^2\left(\Delta_1 + \Delta_2 + \Delta_3\right) \geq 0, \end{aligned} \tag{5.32}$$

with equality iff (5.29) holds. The $\{\Delta_i\}$ for the sum on the RHS of (5.32) are found in (5.20, 23, 26).

Note that the mathematical expressions in (5.20, 26) indicate that the penalty for differences between $S_1(f)$ and $S_2(f)$ is particularly severe near spectral peaks of either waveform, which tends to magnify the differences. This would suggest that waveforms having flat spectra might be advantageous. Also, note that Δ_2 can be kept low by just keeping $S_1^2(f)$ and $S_2^2(f)$ proportional, which might be advantageous, if feasible.

The result in (5.32) can be converted into lower bounds on λ_2 itself or on (λ_2 / λ_1), using the expression for $H(\phi)$ in (5.2), and recalling that

$$Tr\left[H(\phi)\right] = \lambda_1\left[H(\phi)\right] + \lambda_2\left[H(\phi)\right]. \tag{5.33}$$

The trace is periodic in ϕ, but its average value over ϕ or its maximum value over ϕ are easy to obtain from (5.2).

Because $\Sigma(\phi)$ has only nonnegative eigenvalues, the average of $\lambda_1(\phi)\lambda_2(\phi)$ in (5.32) can be 0 *iff* $\lambda_1(\phi)\lambda_2(\phi) = 0$ for all ϕ. But $\Sigma(\phi)$ is of rank 1 or 0 *iff* $\lambda_1(\phi)\lambda_2(\phi) = 0$. Thus, the result in (5.32) implies the following statement, which is utilized and extended in the next section:

For T = 2, the MIMO clutter covariance $\Sigma(\phi)$ is of rank 1 or 0 for all

ϕ iff the waveforms are proportional. (5.34)

The next section extends this statement to $T > 2$.

This page intentionally left blank.

6. IMPACT OF UNEQUAL WAVEFORMS ON THE SECOND EIGENVALUE OF THE MIMO CLUTTER COVARIANCE, WHEN T > 2

The purpose of this section is to extend (5.34) to $T > 2$. The proof involves two steps. The first step establishes the equivalence of the three mathematical conditions shown in Figure 6.1, regarding the MIMO clutter covariance and the waveform cross-correlation matrix. The second step uses the equivalence of the three conditions to reach the desired result.

The equivalence of Conditions (A–C) will be established by proving, in order, the four implications labeled in Figure 6.1.

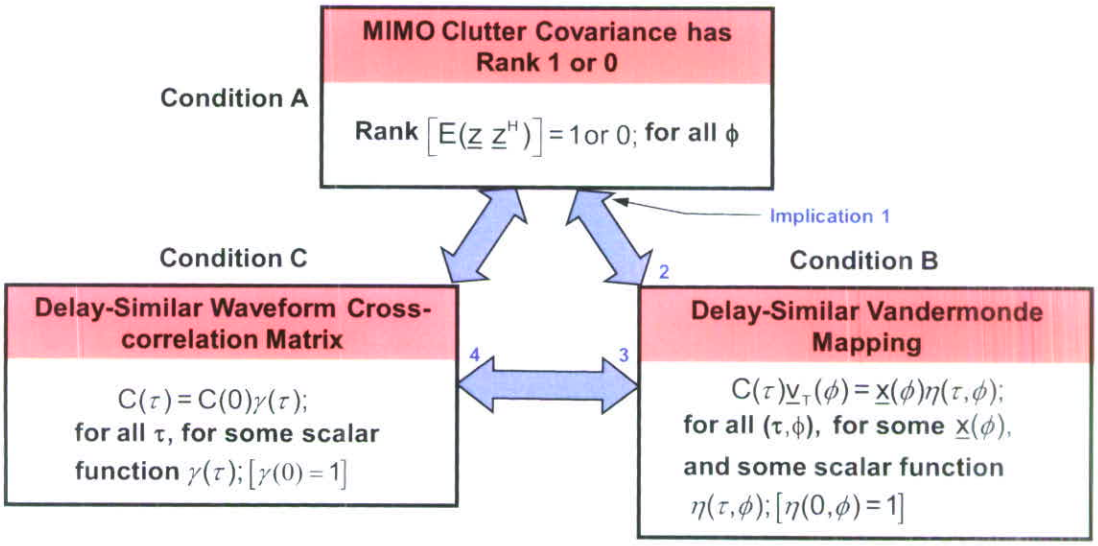

Figure 6.1. Equivalence of conditions.

Proof of Implication 1

Condition B states that

$$C(\tau)\underline{v}_T(\phi) = \underline{x}(\phi)\eta(\tau,\phi); \forall(\tau,\phi), \tag{6.1}$$

where

$$\eta(0,\phi)=1\,. \tag{6.2}$$

Note that (6.1, 2) imply that

$$\underline{x}(\phi)=C(0)\underline{v}_T(\phi). \tag{6.3}$$

Also, note that $\underline{x}(\phi)$ may be $\underline{0}$ for some values of ϕ.

From (3.21, 22) then,

$$H(\phi)=\underline{x}(\phi)\left[\int\left|\eta(\tau,\phi)\right|^2 d\tau\right]\underline{x}^H(\phi), \tag{6.4}$$

so $H(\phi)$ has exactly one nonzero eigenvalue, if $\underline{x}(\phi)$ is not $\underline{0}$ (recall [6.2]), and $H(\phi)$ is a 0 matrix if $\underline{x}(\phi)$ is $\underline{0}$. By (3.25) then, $\Sigma(\phi)$ has less than two nonzero eigenvalues, and thus $\Sigma(\phi)$ has rank 1 or rank 0, establishing Condition A.

Proof of Implication 2

Assume that Condition B is not true. It shall be shown that then Condition A is also not true. Note that $G(\tau,\phi)$ in (3.22) is positive-semidefinite for all (τ,ϕ). But $G(\tau,\phi)$ is the kernel of the integral for $H(\phi)$ in (3.21). If Condition B is not true, then instead of

$$C(\tau)\underline{v}_T(\phi)=\underline{x}(\phi)\eta(\tau,\phi),$$

one would have, for some ϕ_0,

$$C(\tau)\underline{v}_T(\phi_0)=\underline{x}(\tau,\phi_0)\eta(\tau,\phi_0), \tag{6.5}$$

with $\underline{x}(\tau,\phi_0)$ and $\eta(\tau,\phi_0)$ guaranteed to be nonzero for some values of (τ) and with $\underline{x}(\tau,\phi_0)$ guaranteed to change its direction as (τ) varies. But then, in (3.21, 22),

$$H(\phi_0)=\int\underline{x}(\tau,\phi_0)\left|\eta(\tau,\phi_0)\right|^2\underline{x}^H(\tau,\phi_0)\,d\tau\,. \tag{6.6}$$

The integrand is positive-semidefinite, Hermitian; hence, the integral can grow only in the ordering of positive-semidefinite matrices over the integration range of (τ). Because $\underline{x}(\tau,\phi_0)$ changes direction as τ varies, $H(\phi_0)$ must have rank greater than 1, and (3.25) ensures that $\Sigma(\phi_0)$ also has rank greater than 1. Thus, Condition A is not met.

Proof of Implication 3

If Condition C is met, then

$$C(\tau) = C(0)\gamma(\tau);(\forall\tau), \tag{6.7}$$

$$\gamma(0) = 1. \tag{6.8}$$

Then

$$C(\tau)\underline{v}_T(\phi) = C(0)\underline{v}_T(\phi)\gamma(\tau);(\forall\tau). \tag{6.9}$$

To satisfy Condition B, define

$$\underline{x}(\phi) \triangleq C(0)\underline{v}_T(\phi), \tag{6.10}$$

$$\eta(\tau,\phi) \triangleq \gamma(\tau). \tag{6.11}$$

Proof of Implication 4

Condition B gives (6.1, 2). It will be shown that this implies Condition C, which is (6.7, 8). First, by (3.31), the autocorrelation functions $\{c_{nn}(\tau)\}$ satisfy

$$c_{nn}(0) > 0;(n = 1,\ldots,T). \tag{6.12}$$

In (6.3), $\underline{x}(\phi)$ was identified as

$$\underline{x}(\phi) = C(0)\underline{v}_T(\phi). \tag{6.13}$$

One must keep in mind that $\underline{x}(\phi)$ may be $\underline{0}$, for some values of ϕ. Pick an arbitrary value, τ_0, for τ. It will be shown that (6.7) holds for τ_0. Then, (6.8) is a simple consequence of (6.7), proving Condition C, because τ_0 was arbitrary. Substituting (6.13) in (6.1), Condition B implies that

$$C(\tau_0)\underline{v}_T(\phi) = C(0)\underline{v}_T(\phi)\eta(\tau_0,\phi);(\forall\phi). \tag{6.14}$$

Because ϕ is periodic, one can write $\eta(\tau_0,\phi)$ as a Fourier series:

$$\eta(\tau_0,\phi) = \sum_{m=-\infty}^{\infty} \eta_m(\tau_0)e^{jm\phi}. \tag{6.15}$$

Substituting (6.15) into (6.14), one obtains

$$C(\tau_0)\underline{v}_T(\phi) = \left[C(0)\underline{v}_T(\phi)\right]\left[\sum_{m=-\infty}^{\infty} \eta_m(\tau_0)e^{jm\phi}\right];(\forall\phi). \tag{6.16}$$

Consider the nth row of (6.16). On the LHS, one has a sum of complex exponentials, having forms in the set

$$\left\{e^{j0}, e^{j\phi}, \ldots, e^{j(T-1)\phi}\right\}. \tag{6.17}$$

Because (6.14) is assumed to be true, the coefficients $\{\eta_m(\tau_0)\}$ must result only in frequencies on the RHS of (6.16) that are included in the set (6.17). This must hold for every row of (6.16) (i.e., for all n).

Consider the first factor in brackets on the RHS of (6.16). In the nth row of this vector, the coefficient of $\exp\left[j(n-1)\phi\right]$ is $c_{nn}(0)$, which is positive, per (6.12). Thus, if one chooses $(n=1)$, the coefficient of $\exp[j0\phi]$ is $c_{11}(0)$. In order not to generate frequencies outside of (6.17), it is necessary that

$$\eta_m(\tau_0) = 0 \; ; \; m < 0. \tag{6.18}$$

Now, let (n = T). One concludes similarly that

$$\eta_m(\tau_0) = 0 \; ; \; m > 0. \tag{6.19}$$

Thus, only $\eta_0(\tau_0)$ can be nonzero, so from (6.16)

$$C(\tau_0)\underline{v}_T(\phi) = C(0)\underline{v}_T(\phi)\eta_0(\tau_0); (\forall \phi). \tag{6.20}$$

This must be true for all τ, because τ_0 was arbitrary.

Finally, one may pick $\{\phi_1, \ldots, \phi_T\}$ to yield a Vandermonde basis for $\mathbb{C}^T$:

$$\left[\underline{v}_T(\phi_1), \ldots, \underline{v}_T(\phi_T)\right] \triangleq V. \tag{6.21}$$

Then, by (6.20)

$$C(\tau)V = C(0)V\eta_0(\tau); (\forall \tau), \tag{6.22}$$

and one can postmultiply by V^{-1} to obtain

$$C(\tau) = C(0)\eta_0(\tau); (\forall \tau). \tag{6.23}$$

To obtain (6.7), one merely identifies

$$\gamma(\tau) = \eta_0(\tau). \tag{6.24}$$

Recall that (6.7) implies (6.8), so Condition C has been proven, when Condition B was assumed. Thus, implications 1–4 have been established. The equivalence of Conditions A–C follows. In an aside, the fact that Condition A implies Condition C is another way of looking at why uncorrelated signals cannot support good clutter cancellation. As noted in (3.37), uncorrelated signals also have very mismatched autocorrelation function shapes, making their waveform correlation matrices not delay similar. Thus, Condition C does not hold, and hence Condition A cannot hold. Also, the fact that Condition C implies Condition A tells why ideal waveforms would have yielded a rank 1 or rank 0 MIMO clutter covariance, if such waveforms had existed over extended range domains. This explains the good SINR performance

shown in Section 1, for simulated ideal waveforms. In fact, when ideal waveforms were simulated, C(0) was forced to equal I_T, so that in Condition C

$$C(\tau) = I_T \gamma(\tau); (\forall \tau), \tag{6.25}$$

and thus in (3.22),

$$G(\tau, \phi) = \underline{v}_T(\phi) |\gamma(\tau)|^2 \underline{v}_T^H(\phi). \tag{6.26}$$

Then in (3.21),

$$H(\phi) = \underline{v}_T(\phi) \left[\int |\gamma(\tau)|^2 \, d\tau \right] \underline{v}_T^H(\phi), \tag{6.27}$$

and in (3.20), using (3.19),

$$\begin{aligned} \Sigma(\phi) &= B(\phi) \underline{v}_T(\phi) \left[\int |\gamma(\tau)|^2 \, d\tau \right] \underline{v}_T^H(\phi) B^H(\phi) \\ &= \left[\underline{v}_R(\phi) \otimes I_T \right] \underline{v}_T(\phi) \left[\int |\gamma(\tau)|^2 \, d\tau \right] \underline{v}_T^H(\phi) \left[\underline{v}_R^H(\phi) \otimes I \right] \\ &= \left[1, e^{j\phi}, ..., e^{j(RT-1)\phi} \right]^T \left[\int |\gamma(\tau)|^2 \, d\tau \right] \left[1, e^{j\phi}, ..., e^{j(RT-1)\phi} \right]^*. \end{aligned} \tag{6.28}$$

Thus, the MIMO clutter covariance for ideal waveforms involves the Vandermonde structure for the (single) steering vector of the clutter ray. This further explains the narrowness of the notch in the SINR performance as the velocity of the target changes, making ϕ in (6.28) vary away from ϕ_t in (3.15), for the (Vandermonde) target signature. This is the same sharpness that would be achieved for a SIMO system using real receivers at all the locations of the MIMO virtual array elements, as discussed in the text for Figure 1.4. Note that the structure of $\Sigma(\phi)$ in (6.28) effectively would be the same whether the transmitters or receivers were spaced close together. This is why the SINR performances of these three designs are the same, as mentioned in the text discussion of Figure 1.4.

It is now shown that (5.34) can be extended to T > 2. First, if the T waveforms are all proportional, then all the $c_{ij}(\tau)$ are all proportional autocorrelation functions. Trivially, Condition C is met, and hence Condition A is met, by the equivalence of conditions. Next, if any pair of the T waveforms are not

proportional, then one knows that if these were the only two transmitted waveforms, the MIMO clutter covariance would not be of rank 1 for all ϕ, by (5.34)[7]. But then Condition A of Figure 6.1 would not hold for T = 2. Consequently, Condition C would not hold for T = 2, by the equivalence of conditions. However, the waveform correlation matrix for T = 2 is a subset of that for the full T; hence, Condition C would fail for the full T. Thus, Condition A would fail for the full T. So, one can extend (5.34) to say that

For any T, the MIMO clutter covariance $\Sigma(\phi)$ is of rank 1 or 0

for all ϕ iff all T waveforms are proportional.

(6.29)

This extends the result of (5.34) to $T \geq 2$. However, using the properties of analytic functions it is possible to strengthen (6.29) (and (5.34) by implication) in terms of their applicability over the domain of ϕ. First, one writes (6.29) as a pair of statements

For any T, if all T waveforms are proportional, then the MIMO clutter

covariance $\Sigma(\phi)$ is of rank 1 or 0 for all ϕ. (6.30a)

and

For any T, if any pair of the T waveforms are not proportional,

then the MIMO clutter covariance $\Sigma(\phi)$ must have rank >1 for

some value of ϕ. (6.30b)

Below, (6.30b) will be strengthened to read:

---

[7] Note that the potential increase in spacing above $\lambda/2$ for two arbitrary transmitters has no impact on the relevant proofs, because the proofs dealt directly with ϕ from (3.1).

For any T, if any pair of the T waveforms are not proportional, then the MIMO clutter covariance $\Sigma(\phi)$ can have rank 1 or 0 only for isolated values of ϕ. (6.31)

The following argument was obtained from Keith Forsythe of Lincoln Laboratory [19]. It is first noted that all the elements of the $\Sigma(\phi_c)$ are analytic in ϕ_c, where ϕ_c is obtained by adding an imaginary part to ϕ, which is a real variable. This fact follows immediately, because these elements are all just sums of complex exponentials in ϕ_c, as shown by (3.14, 19, 20, 42).

Next, it is noted that a complex matrix W can be Hermitian and of rank 1 or 0 iff

$$W = \underline{w}\,\alpha\,\underline{w}^H;(\textit{for some complex vector } \underline{w} \textit{ and real scalar } \alpha). \tag{6.32}$$

This is true via eigendecomposition. It is shown next that (6.32) is equivalent to the two following sets of conditions on W.

$$g_{i,j}(W) \triangleq W_{ij} - W_{ji}^* = 0; \forall(i,j), \tag{6.33}$$

$$h_{j,k,\ell,m}(W) \triangleq W_{jk}W_{\ell m} - W_{jm}W_{\ell k} = 0; \forall(j,k,\ell,m). \tag{6.34}$$

The functions $\{h_{j,k,\ell,m}(\cdot)\}$ are analytic in their arguments. The $\{g_{i,j}(\cdot)\}$ are not analytic functions, but that won't matter below. The fact that (6.32) implies (6.33, 34) is easy to show. First, (6.33) just says that W is Hermitian, which is implied by (6.32). Second, (6.32) implies that

$$\begin{aligned} W_{jk}W_{\ell m} - W_{jm}W_{\ell k} &= \left(w_j w_k^* w_\ell w_m^* - w_j w_m^* w_\ell w_k^*\right)\alpha^2 \\ &= 0; (\forall j,k,l,m), \end{aligned} \tag{6.35}$$

proving (6.34). Next, it is shown that (6.33, 34) imply (6.32). The proof requires a few steps. Consider any complex matrix W satisfying (6.33, 34). If W = 0, then (6.32) is met when $\alpha = 0$. So say that $W \neq 0$, so $\alpha \neq 0$. If the elements of the n^{th} column of W are all 0, then (6.33) implies that the elements of the n^{th} row of W are also all 0. The union of that row and column, which has the shape of the crossing of a

horizontal line with a vertical line within W, satisfies the condition in (6.32), with w_n set to 0. Thus, one may remove that column and row from W, and consider whether (6.32) is met for the remainder of the matrix. Assume that W now has had all such $\underline{0}$ columns and corresponding $\underline{0}$ rows removed. Thus, every column of W now has some nonzero entry.

One may now show that the reduced matrix W in fact has no zero entries. Suppose that element W_{jk} is 0. One can then obtain a contradiction. It is known that the k^{th} column also contains a nonzero element—call it $W_{\ell k}$. Pick an arbitrary column, ($m \neq k$). It is known from (6.34) that

$$W_{jk} W_{\ell m} = W_{jm} W_{\ell k}. \tag{6.36}$$

The LHS is 0 if $W_{jk} = 0$, and it is known that $W_{\ell k}$ is nonzero, so W_{jm} is 0. Thus, the entire j^{th} row is 0. By (6.33), the entire j^{th} column is also 0. But this row and column would have been removed in the initial reduction of W, which is a contradiction. So, the reduced W has no zero entries.

Because the reduced W has no zero entries, one may now consider arbitrary (j,k,ℓ,m) and examine the implications of (6.36). If one divides both sides by $W_{\ell k} W_{\ell m}$ (which cannot equal 0), one obtains

$$\frac{W_{jk}}{W_{\ell k}} = \frac{W_{jm}}{W_{\ell m}}. \tag{6.37}$$

As this equality ranges over j and ℓ, it shows that the k^{th} and m^{th} columns are proportional. Because k and m were arbitrary, all columns are proportional, and W is of rank 1. But (6.33) said that W was Hermitian, so it must have the form in (6.32) for its eigendecomposition. This establishes the equivalence of (6.32) to (6.33, 34).

One may now return to strengthening (6.30b). When any pair of the T waveforms are not proportional, (6.30b) says that $\Sigma(\phi)$ must have rank >1 for some value of ϕ. Consider such a value of ϕ. Then $\Sigma(\phi)$ cannot be written as in (6.32), and hence (6.33, 34) cannot all be true. However, $\Sigma(\phi)$ is Hermitian, so (6.33) is true. Thus, (6.34) must be violated. In other words,

$$h_{j,k,\ell,m}\left[\Sigma(\phi)\right] \neq 0; \; for \; some(j,k,\ell,m). \tag{6.38}$$

Extending ϕ to complex ϕ_c, (6.38) says that for some ϕ_c on the real axis

$$h_{j,k,\ell,m}\left[\Sigma\left(\phi_c\right)\right] \neq 0; \textit{ for some}\left(j,k,\ell,m\right). \tag{6.39}$$

But the composite functions of ϕ_c in (6.39) are all analytic in ϕ_c, because all elements of $\Sigma\left(\phi_c\right)$ are analytic in ϕ_c. Thus, if any of these functions is not zero for a point in the complex plane, then it can only be 0 at isolated points in the plane [26, pp. 739–743], hence only at isolated points on the real axis (which means real ϕ values). Because of the equivalence of (6.33, 34) to (6.32), one sees that (6.32) can be true only for $\Sigma\left(\phi\right)$ for isolated values of ϕ. But (6.32) is equivalent to $\Sigma\left(\phi\right)$ being Hermitian, of rank 1 or 0. However, it is already known that $\Sigma\left(\phi\right)$ is Hermitian (3.20), so $\Sigma\left(\phi\right)$ can only be of rank 1 or 0 for isolated values of ϕ. Condition (6.31) follows, as desired.

7. PROSPECTS FOR IMPROVING THE CANCELLATION OF CLUTTER OVER EXTENDED DOMAINS

This section briefly discusses three different potential techniques for improving the cancellation of clutter over extended domains. The techniques are adaptively weighted slow-time taps (i.e., Space-Time Adaptive Processing, or STAP [18]), adaptively weighted fast-time taps, and nonconventional reception (that is, reception not assuming the use of matched filters for the T waveforms). The discussion focuses on the case of uncorrelated waveforms, as considered in Section 4. A more comprehensive treatment of this subject would consider the joint problem of waveform design together with the processing options listed above.

STAP is examined first, for the case of repetitive, pulsed-Doppler waveforms. The SINR performance examples given in the text utilized two pulse-repetition-interval (PRI) staggers [18, p. 125]. One could consider adding more staggers, or utilizing fully adaptive STAP. In the latter case, for the hypothesized range cell of the target, the sampled matched-filter outputs lie in the (3-D) domain of (antenna number, MF number, pulse number). Consider the following question. For uncorrelated pulse waveforms, will any of the outputs in the 2-D domain of (antenna number, pulse number) for MF#k have any correlation with any of the outputs for MF#m, for $k \neq m$? The answer is no, as is now discussed. In Section 4, the discussion considered only clutter on the target isoDop. However, note that $H(\phi)$ in (4.4) is a scaled identity matrix for all values of ϕ. Hence, for each pulse alone, with no preDoppler filtering, one can conclude (similarly to the discussion at the end of Section 4) that the processed antenna outputs for MF#k are all uncorrelated with those for MF#m, unless $k = m$. For short coherent processing intervals, the cross-correlation gain patterns—see (3.17)—on the ground corresponding to the various combinations of transmit waveforms and MF numbers do not change significantly for different pulses. Thus, it is clear that there will be little correlation between any of the outputs in the 2-D domain of (antenna number, pulse number) for MF#k with any of those for MF#m, unless $k = m$. Hence, the 2-D domain of outputs for each matched-filter number must be weighted to form its own null, which effectively increases the required number of degree of freedom for clutter cancellation. Consequently, fully adaptive STAP is not expected to restore ideal SINR performance.

Adaptive weighting of fast-time taps at the MF outputs is now examined. In this case, the MF outputs would no longer be sampled only at the hypothesized target range, but also at other ranges in the vicinity of the hypothesized target range, for adaptive weighting. The adaptive weighting would be over the domain of (antenna number, MF number, range sample). The concept of the argument here is similar to that for slow-time taps. For uncorrelated waveforms, the question is whether any of the outputs in the (2-D) domain of (antenna number, range sample) for MF#m will have any correlation with any of the outputs for MF#n, when $m \neq n$. The answer is no, as shown below. Return to considering only the clutter on the isoDop to the hypothesized target. For any specific range sample, including the target range, the argument at the end of Section 4 shows that the antenna outputs for MF#m are all uncorrelated with those for MF#n, unless $m = n$. However, one must now consider the correlations between samples at different

ranges and MF outputs. This requires some modifications to the previous derivation. The MF outputs at the target range were expressed in (3.17), which is repeated here.

$$\underline{z} = \left[\underline{v}_R(\phi) \otimes I_T \right] \int C(\tau) \underline{v}_T(\phi) u(\tau) d\tau . \tag{7.1}$$

The discussion in Section 3 considered the covariance of $\underline{z}$. Now one must examine the cross-correlation of $\underline{z}$ and $\underline{z}_\varepsilon$, where ε is a time offset corresponding to sampling the MFs at a range somewhat offset from that of the target. The impact of the sample-time offset is to offset $s_k(\cdot)$ in (3.6), resulting in an offset of the gain pattern, $C(\tau)$, being put on the clutter on the isoDop. Thus, similar to (7.1),

$$\underline{z}_\varepsilon = \left[\underline{v}_R(\phi) \otimes I_T \right] \int C(\tau + \varepsilon) \underline{v}_T(\phi) u(\tau) d\tau. \tag{7.2}$$

One must examine the cross-correlation between $\underline{z}$ and $\underline{z}_\varepsilon$:

$$\Sigma_\varepsilon(\phi) \triangleq E\left[\underline{z} \underline{z}_\varepsilon^H \right]. \tag{7.3}$$

Analogous to (3.20–22), one obtains here

$$\Sigma_\varepsilon(\phi) = B(\phi) H_\varepsilon(\phi) B^H(\phi), \tag{7.4}$$

where

$$H_\varepsilon(\phi) \triangleq \int G_\varepsilon(\phi, \tau) d\tau, \tag{7.5}$$

and

$$G_\varepsilon(\phi, \tau) \triangleq C(\tau) \underline{v}_T(\phi) \underline{v}_T^H(\phi) C^H(\tau + \varepsilon). \tag{7.6}$$

The key step is to modify the expressions in (3.28, 29), to account for the sample-time offset:

$$\int c_{ij}(\tau)c_{kl}^{*}(\tau+\varepsilon)\,d\tau$$
$$= \int\Big[\int S_i^{*}(f)S_j(f)\exp\{j2\pi f\tau\}\,df\Big]\Big[\int S_k^{*}(\gamma)S_\ell(\gamma)\exp\{j2\pi\gamma(\tau+\varepsilon)\}\,d\gamma\Big]^{*}\,d\tau$$
$$= \iint S_i^{*}(f)S_j(f)S_k(\gamma)S_\ell^{*}(\gamma)\Big[\int\exp\{j2\pi(f-\gamma)\tau\}\,d\tau\Big]\exp\{-j2\pi\gamma\varepsilon\}\,df\,d\gamma$$
$$= \int S_i^{*}(f)S_j(f)S_k(f)S_\ell^{*}(f)\exp\{-j2\pi f\varepsilon\}\,df \tag{7.7}$$

$$\triangleq \Phi_{ijk\ell}(\varepsilon). \tag{7.8}$$

One obtains, analogously to (3.41),

$$\big[G_\varepsilon(\phi,\tau)\big]_{mn} = \sum_{k=1}^{T}\sum_{i=1}^{T}c_{mi}(\tau)c_{nk}^{*}(\tau+\varepsilon)\exp\{j\phi(i-k)\}, \tag{7.9}$$

and from (7.5, 8) one has

$$\big[H_\varepsilon(\phi)\big]_{m,n} = \sum_{k=1}^{T}\sum_{i=1}^{T}\exp\{j\phi(i-k)\}\,\Phi_{mink}(\varepsilon). \tag{7.10}$$

But for uncorrelated waveforms, (3.36) showed that the waveforms share no frequency support. Thus, by (7.7) one has analogously to (4.1) that

$$\Phi_{mink}(\varepsilon) = 0,\ unless\ m = i = n = k. \tag{7.11}$$

Thus, similarly to (4.2),

$$\big[H_\varepsilon(\phi)\big]_{m,n} = \begin{pmatrix} T\Phi_{mmmm}(\varepsilon); & m = n \\ 0; & otherwise \end{pmatrix};(\forall\phi). \tag{7.12}$$

If one substitutes (7.12) into (7.4) and uses (3.19), one finds that

$$\begin{aligned}\Sigma_{\varepsilon}(\phi) &= \left[\underline{v}_R(\phi)\otimes \underline{I}_T\right] diag\left(T\Phi_{mmmm}(\varepsilon)\right)\left[\underline{v}_R^H(\phi)\otimes \underline{I}_T\right] \\ &= \left[\underline{v}_R(\phi)\otimes \underline{I}_T\right]\left[1\otimes diag\left(T\Phi_{mmmm}(\varepsilon)\right)\right]\left[\underline{v}_R^H(\phi)\otimes \underline{I}_T\right] \\ &= \left[\underline{v}_R(\phi)\underline{v}_R^H(\phi)\right]\otimes diag\left(T\Phi_{mmmm}(\varepsilon)\right). \end{aligned} \tag{7.13}$$

This expression implies that none of the antenna output samples for MF#m correlate with any for MF#n, whatever the time shift between samples. Thus, cancellation of the clutter must use weights that cancel the antenna outputs from MF#m (with some benefit from extra range samples, perhaps) and also cancel the outputs from MF#n. This requires extra degrees of freedom and indicates that adaptive weighting of extra fast-time samples should not be expected to restore ideal performance.

Consideration is now given to nonconventional receiver processing, where this term refers to processing not assuming the use of matched filtering. Consider the case of a pulsed-Doppler waveform. The clutter data for each antenna element can be likened to the data measured for SAR imaging, and can be considered to lie in the 2-D (fast frequency, pulse number) domain, with its 2-D Fourier transform being the (range, Doppler) SAR image domain. Consider the data for one antenna in the (fast frequency, pulse number) domain. For the case of uncorrelated pulse waveforms, it is known that the waveforms do not share spectral support in the fast-frequency domain (see (3.36)). For the m^{th} transmitter, the measured data in the frequency-support region has the frequency response $S_m(f)$ (here referring to a single pulse) imposed by the transmitter. Imagine that the data for each antenna was reversibly normalized, conceptually, by multiplying it by $\left[S_m^*(f)/|S_m(f)|^2\right]$, and that this was done separately for each transmitter's support region in frequency. If the data were Doppler filtered to the Doppler frequency of the hypothesized target, each antenna element would just have data in the fast-frequency domain corresponding to clutter on the isoDop to the target. The overall data would thus lie in the 2-D (fast frequency, antenna element) domain. Because the isoDop is just a ray in cone angle off the platform motion direction, it can clearly be cancelled by weighting the antenna-element domain samples at each frequency, producing nulls at each frequency, along the isoDop. However, to get cancellation by combining data from different frequencies is another matter. Because the clutter can be modeled as white in reflectivity, the clutter along a long ray in range on the ground induces (through the Fourier transform) a correlation function that is very narrow in the transform domain of fast frequency. Hence, samples for different transmitters (at different frequencies) will not correlate well. Thus, clutter cancellation will not be able to rely on combining data from different transmitters. This suggests that the nonconventional receiver approach also fails to address the basic problem for uncorrelated pulse signals, while it still may improve performance somewhat.

8. BENEFITS OF A LIMITED RANGE-DOPPLER DOMAIN OF CLUTTER

As discussed in Section 2, the results in Sections 3–7 were generated under the assumption of an extended range domain of clutter. Of course, the earth is of finite extent, and the antenna-element footprints on the ground may be of much lesser extent, both in range and azimuth. Further, for monostatic radars the return power for a constant scattering area on the ground falls off as $(r_0 + r)^{-4}$, where $(r_0 + r)$ is the slant range of the scattering region—recall that r was defined in (3.3) as the offset of the range of a clutter patch from that of the hypothesized target at range r_0. Under some circumstances, these factors dramatically impact the achievable SINR performance, for appropriately chosen waveforms. It is well known that waveform sets such as time-division multiple access (TDMA) are able to yield near-ideal performance with clutter having a suitably limited range domain. Here, it will be shown how this fact relates to the analysis of the extended-domain case performed in the previous sections. The discussion will treat only TDMA, although a number of different types of waveform sets are also able to exploit finite domains of clutter [3, 15].

The discussion here assumes a basic pulsed-Doppler radar waveform design. Each transmitter emits a pulse of duration T_p seconds, every T_r seconds. The transmitters are interleaved in time, as shown in Figure 8.1. Thus, for T transmitters there is a time spacing of (T_r / T) between pulse start-times. All pulses sent by all transmitters during the coherent processing interval are identical in modulation. The autocorrelation functions of all T waveforms are thus identical, also shown in Figure 8.1. However, the cross-correlation functions are quite dissimilar, as also shown there. The key fact is that within the time delay of $\left[(T_r / T) - T_p\right]$, the cross-correlation functions are all 0; hence the waveform correlation matrix $C(\tau)$ is delay similar, over the interval

$$|\tau| \le (T_r / T) - T_p . \tag{8.1}$$

This says that Condition C of Section 6 holds over this interval of τ. Going back to the derivation of the equivalence of Conditions A–C in Section 6, one may observe that those derivations applied for clutter having any domain of τ. Thus, Condition A also holds, so that the MIMO covariance is of rank 1 or 0 for all values of ϕ, provided that the clutter returns are within the domain in (8.1). If the clutter extends beyond the domain in (8.1), then the rank grows beyond 1. However, if the clutter outside the domain is weak enough (e.g., due to $(r_0 + r)^{-4}$ losses or a limited antenna elevation footprint), then the extended clutter will not be of operational significance, being too weak to require good cancellation.

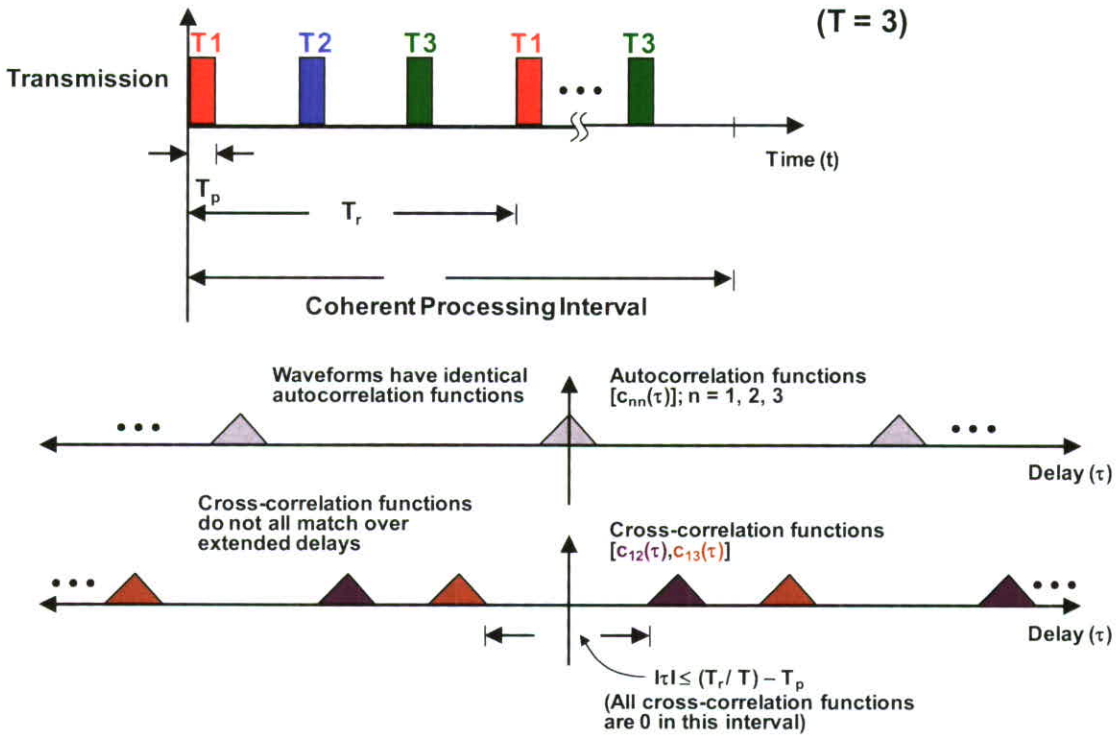

Figure 8.1. TDMA waveforms and correlation functions.

Briefly stated, the system design tradeoff to use TDMA to maintain a low-rank MIMO clutter covariance would be as follows. The azimuthal coverage region of the antennas determines the angular domain over which clutter returns need to be cancelled. Call this $\pm\theta_c$ in off-broadside angle. The Doppler cycle shift pulse-to-pulse for a given receiver element (i.e., the normalized Doppler frequency [18, p. 13]) is given by

$$\varpi = 2v_a(\sin\theta)T_r / \lambda, \tag{8.2}$$

where v_a is the velocity of the platform, and θ is the off-broadside angle of the clutter. To avoid Doppler ambiguities in the coverage region, $|\varpi|$ must be kept below ½. Thus,

$$2v_a\left(\sin\theta_c\right)T_r/\lambda<1/2\,,$$

$$T_r<\frac{\lambda}{4v_a\left(\sin\theta_c\right)}\,. \tag{8.3}$$

(The reason that Doppler ambiguities must be avoided is that these would add rays of clutter to cancel, increasing the rank of the MIMO clutter covariance.) To have a low-rank MIMO covariance matrix using TDMA, the elevation pattern and $\left(r_0+r\right)^{-4}$ falloff must be such that the clutter requiring cancellation is limited in delay, as given in (8.1), with T_r from (8.3). Thus, the applicability of TDMA for maintaining a low-rank MIMO clutter covariance depends on the system design in terms of v_a, λ, the azimuth and elevation coverage region, the number of transmitters, and the duty cycle.

It is useful to note that the TDMA waveforms are specifically chosen to have matching autocorrelation functions, as required to meet Condition C of Section 6, and hence to produce a rank 1 or rank 0 MIMO clutter covariance, via equivalent Condition A of Section 6. The fact that the clutter is range-Doppler limited is not sufficient to obtain good clutter cancellation, unless the waveforms are specifically chosen to exploit that. For example, fully uncorrelated waveforms have orthogonal correlation functions (3.37), which often differ markedly in their primary lobe, in the immediate vicinity of the target. This could cause increased rank of the MIMO covariance even for range-Doppler limited clutter. This argues against the use of waveforms sets (like the Wolf Whistles used in Figure 1.6) that are designed for low cross-correlations at all delays. As the domain of the clutter region increases, the best design of MIMO waveforms for minimal degradation of clutter cancellation while achieving other beneficial properties remains an open issue. Airborne experimental data will be used to assess the resulting performance.

This page intentionally left blank.

9. SUMMARY

The use of uncorrelated waveforms for MIMO GMTI is desirable, because it diffuses the transmit energy over a broad azimuthal coverage region, leading to increased effective coherent integration time. Unfortunately, as has been observed in computer simulations and now analyzed herein, when the clutter occupies an extended domain of delay, the clutter cancellation achieved by using practical, low-correlation sets of waveforms is significantly worse than that for ideal uncorrelated waveforms (i.e., uncorrelated waveforms having matching autocorrelation functions). Such ideal sets of waveforms do not exist over extended domains of delay (they do exist for suitably limited domains of delay). For extended domains of delay, actual uncorrelated waveforms must have nonoverlapping frequency support (3.36), giving them orthogonal autocorrelation functions (3.37). The clutter on the ground is weighted by these autocorrelation functions, causing a loss of correlation in the MIMO clutter covariance. It is proven in Section 4 that for T uncorrelated transmitters the MIMO clutter covariance matrix has T equal, positive eigenvalues, causing clutter cancellation problems. (For a single transmitter, the rank of the comparable clutter covariance matrix is 1 or 0—see 3.39.) The outputs of the matched filters corresponding to each transmitter are uncorrelated with the outputs for all other transmitters, as seen at the various receiver outputs. Thus, the clutter cancellation is performed only by the receivers (Section 4). For a critically spaced virtual array, if the receivers are closer together than the transmitters, then the notch in the SINR loss versus hypothesized target velocity is wider than the ideal case. If the receivers are farther apart, multiple narrow notches are experienced, because of array ambiguities. In effect, the dependence of clutter nulling on the receive array design would thus be the same for MIMO as for SIMO.

If the waveforms are allowed to be somewhat correlated, it was shown in Section 6 that if any pair of the T transmitters are not proportional, then the rank of the MIMO clutter covariance must be greater than 1 for all but isolated values of the direction of the clutter-ray isoDoppler to the hypothesized target. For the special case of $T = 2$, the average value of the product of the top two eigenvalues of the MIMO clutter covariance was shown (in Section 5) to have a quadratic penalty whenever the waveforms are not proportional. Unfortunately, the penalty emphasizes differences between waveforms at the frequencies where either waveform is most powerful. This suggests the use of flat-spectrum waveforms.

A brief discussion was given in Section 7 of the potential benefits of adaptively weighting either slow-time taps (i.e., STAP) or fast-time taps. Also, the potential use of receivers that do not employ matched filters for the waveforms was considered. It was found that the fundamental problem caused by the use of uncorrelated signals is not addressed by any of these techniques, although some performance improvements might be obtained.

For limited domains of clutter in range Doppler, the example of TDMA waveforms was considered, showing how they could yield ideal performance in the context of the analysis done herein. The system parameter requirements for ideal performance with this waveform type were discussed. The antenna coverage footprint in azimuth and range on the ground are important, as well as the platform velocity, the

center frequency, and the duty cycle (Section 8). As the domain of the clutter grows, the best design of MIMO waveforms for minimal degradation of clutter cancellation and other beneficial properties remains an open issue. Airborne experimental data will be used to assess the resulting performance.

REFERENCES

1. K.W. Forsythe and D.W. Bliss, *Signal Processing for MIMO Radar*, John Wiley and Sons, Inc., 2008, ch. MIMO Radar: Concepts, Performance Enhancements, and Applications.

2. V.F. Mecca, J.L. Krolik, and F.C. Robey, "Beamspace Slow-Time MIMO Radar for Multipath Clutter Mitigation," *IEEE Intl. Conference on Acoustics, Speech and Signal Processing, ICASSP 2008*, pp. 2313–2316.

3. D.W. Bliss, K.W. Forsythe, S.K. Davis, G.S. Fawcett, D.J. Rabideau, L.L. Horowitz, and S. Kraut, "GMTI MIMO Radar," *IEEE Waveform Diversity and Design Conference*, 2009, pp. 118–122.

4. I. Bekkerman and J. Tabrikian, "Target Detection and Localization Using MIMO Radars and Sonars," *IEEE Transactions on Signal Processing*, 2006, pp. 3873–3883.

5. J. Tabrikian, "Barankin Bounds for Target Localization by MIMO Radars," *IEEE Workshop on Sensor Array and Multichannel Processing*, 2006, pp. 278–281.

6. S. Coutts, K. Cuomo, J. McHarg, F. Robey, and D. Weikle, "Distributed Coherent Aperture Measurements for Next Generation BMD Radar," *IEEE Workshop on Sensor Array and Multichannel Processing*, 2006, pp. 390–393.

7. K.W. Forsythe and D.W. Bliss, "Waveform Correlation and Optimization Issues for MIMO Radar," *Asilomar Conference on Signals, Systems and Computers*, 2005, pp. 1306–1310.

8. K.W. Forsythe, D.W. Bliss, and G.S. Fawcett, "Multiple-Input Multiple-Output (MIMO) Radar: Performance Issues," *Asilomar Conference on Signals, Systems and Computers*, 2004, pp. 310–315.

9. D.W. Bliss and K.W. Forsythe, "Multiple-Input Multiple-Output (MIMO) Radar and Imaging: Degrees of Freedom and Resolution," *Asilomar Conference on Signals, Systems and Computers*, 2003, pp. 54–59.

10. F.C. Robey, S. Coutts, D. Weikle, J.C. McHarg, and K. Cuomo, "MIMO Radar Theory and Experimental Results," *Asilomar Conference on Signals, Systems and Computers*, 2004, pp. 300–304.

11. D.J. Rabideau and P. Parker, "Ubiquitous MIMO Multifunction Digital Array Radar," *Asilomar Conference on Signals, Systems and Computers*, 2003, pp. 1057–1064.

12. H.A. Kahn and D.J. Edwards, "Doppler Problems in Orthogonal MIMO Radars," *IEEE Radar Conference*, 2006, pp. 244–247.

13. Bo Liu, Z. He, J. Zeng, and B. Liu, "Polyphase Orthogonal Code Design for MIMO Radar Systems," *CIE Intl. Conference on Radar*, 2006, pp. 1–4.

14. H. Deng, "Polyphase Code Design for Orthogonal Netted Radar Systems," *IEEE Transactions on Signal Processing*, 2004, pp. 3126–3135.

15. D.J. Rabideau, "Adaptive MIMO Radar Waveforms," *IEEE Radar Conference*, 2008, pp. 1349–1354.

16. S.K. Davis and G.S. Fawcett, MIT Lincoln Laboratory, private communication, 2008.

17. A.W. Rihaczek, *Principles of High-Resolution Radar*, Peninsula Publishing, 1985.

18. J. Ward, "Space-Time Adaptive Processing for Airborne Radar," MIT Lincoln Laboratory Technical Report TR-1015, 1994.

19. K.W. Forsythe, MIT Lincoln Laboratory, private communication, 2008.

20. J.V. DiFranco and W.L. Rubin, *Radar Detection*, Prentice-Hall, Inc., 1968.

21. A. Graham, *Kronecker Products and Matrix Calculus With Applications*, John Wiley and Sons, Inc., 1981.

22. C.W. Helstrom, *Statistical Theory of Signal Detection*, Pergamon Press, 1968.

23. D.V. Sarwate and M.B. Pursley, "Crosscorrelation Properties of Pseudorandom and Related Sequences," *Proceedings of the IEEE*, 1980, pp. 593–619, correction on p. 1554.

24. D.V. Sarwate, "Bounds on Crosscorrelation and Autocorrelation of Sequences," *IEEE Transactions on Information Theory*, 1979, pp. 720–724.

25. D.G. Luenberger, *Optimization by Vector Space Methods*, John Wiley and Sons, Inc., 1969.

26. Kiyosi Ito, Ed., *Encyclopedic Dictionary of Mathematics*, MIT Press, 1993.

REPORT DOCUMENTATION PAGE

Form Approved
OMB No. 0704-0188

1. REPORT DATE	2. REPORT TYPE	3. DATES COVERED *(From - To)*
31 August 2011	Technical Report	

4. TITLE AND SUBTITLE
Clutter Cancellation Limits of Adaptive Processing Applied to Coherent Multiple-Input Multiple-Output Ground Moving Target Indication

5a. CONTRACT NUMBER
FA8721-05-C-0002

5b. GRANT NUMBER

5c. PROGRAM ELEMENT NUMBER

6. AUTHOR(S)
Larry L. Horowitz

5d. PROJECT NUMBER
1977-22

5e. TASK NUMBER

5f. WORK UNIT NUMBER

7. PERFORMING ORGANIZATION NAME(S) AND ADDRESS(ES) AND ADDRESS(ES)
MIT Lincoln Laboratory
244 Wood Street
Lexington, MA 02420-9108

8. PERFORMING ORGANIZATION REPORT NUMBER
TR-1132

9. SPONSORING / MONITORING AGENCY NAME(S) AND ADDRESS(ES)
Dept. of the Air Force
ESC/CAA
20 Schilling Circle
Hanscom AFB, MA 01731

10. SPONSOR/MONITOR'S ACRONYM(S)

11. SPONSOR/MONITOR'S REPORT NUMBER(S)
ESC-TR-2007-075

12. DISTRIBUTION / AVAILABILITY STATEMENT
Approved for public release; distribution is unlimited.

13. SUPPLEMENTARY NOTES

14. ABSTRACT

For applications in which the geometry and radar system design result in ground clutter occupying a suitably limited extent of range and Doppler, waveform sets such as time-division multiple access (TDMA) or Doppler-division multiple access (DDMA) can be used to achieve near-ideal clutter cancellation performance for coherent, multiple-input multiple-output (MIMO) ground moving target indication (GMTI). However, it has been noted that the clutter cancellation is poorer when the clutter has a greater range-Doppler extent. Various alternative waveform sets have failed to mitigate this problem.

This report shows analytically that the extra difficulty of clutter cancellation is attributable to an unavoidable increase in the number of degrees of freedom required by MIMO to cancel the ground clutter, when the clutter occupies an extended domain of range Doppler. For example, for any set of T uncorrelated signals, under simple assumptions the MIMO virtual spatial covariance matrix for the clutter in the target Doppler bin will have T equal, positive eigenvalues. This is in contrast to the case of clutter occupying a suitably limited domain of range Doppler, where the rank of this MIMO clutter covariance can be forced to be 1 or 0, through proper waveform selection, such as TDMA or DDMA.

15. SUBJECT TERMS

16. SECURITY CLASSIFICATION OF:			17. LIMITATION OF ABSTRACT	18. NUMBER OF PAGES	19a. NAME OF RESPONSIBLE PERSON
a. REPORT	b. ABSTRACT	c. THIS PAGE			19b. TELEPHONE NUMBER *(include area code)*
Unclassified	Unclassified	Unclassified	Same as report	70	

This page intentionally left blank.